# NATIONAL ADVISORY COMMITTEE FOR AERONAUTICS

# WARTIME REPORT

ORIGINALLY ISSUED
February 1942 as
Advance Restricted Report

WIND-TUNNEL INVESTIGATION OF CARBURETOR-AIR INLETS

By W. J. Nelson and K. R. Czarnecki

Langley Memorial Aeronautical Laboratory
Langley Field, Va.

# NACA

WASHINGTON

# WIND-TUNNEL INVESTIGATION OF CARBURETOR-AIR INLETS

## By W. J. Nelson and K. R. Czarnecki

### INTRODUCTION

An investigation of the internal and external air-flow characteristics of carburetor-air inlets for liquid-cooled engine installations has been conducted in the NACA full-scale wind tunnel. Increased airplane speeds and higher operational altitudes have augmented the difficulties in the design of air inlets that are efficient over the entire flight range. Efficient inlets provide a uniform velocity distribution at the carburetor metering venturi with high ramming pressure and a low external drag.

Full-scale models of two representative pursuit airplanes were used in the investigation of nine carburetor-air inlets differing in shape, size, and location. The inlet positions were confined to the forward section of the fuselage. The effects of propeller operation on the inlet characteristics were determined for most of the installations. Measurements of velocity distribution, ram, and drag were made at air quantities and angles of attack corresponding to a wide range of flight conditions for each of these inlets.

### APPARATUS AND TESTS

A description of the NACA full-scale wind tunnel and balance used for these tests is given in reference 1. The models were mounted in the test section as shown in figure 1. The principal dimensions of the models are given in figures 2 and 3. A 10-foot-diameter propeller, fitted with cuffs (fig. 4), and driven by an electric motor was used on model A to determine the effect of the slipstream.

The duct system ahead of the nominal carburetor location was made in two sections; one section formed the inlet and the diffuser and the other contained the bend and the connection with the carburetor flange. Changes in the installation during the tests were confined to the inlet and the diffuser. (See figs. 5 to 15.) All the scoops were of conventional design except scoop 5, which twisted so that the inlet was alined with the direction of the slipstream in the high-speed condition.

Since no engine was provided in these models, it was necessary to add a duct replacing the carburetor to provide an adjustable outlet with which to control the air flow through the installation. The duct installation in model A is shown by an isometric drawing in figure 16; in figures 17 and 18 the details of the bends ahead of the carburetor are given for both models.

The increment of drag added by each duct installation was determined from the difference between force measurements on the bare model and on the model with the carburetor-air system installed. These tests were made over a range of lift coefficients from -0.2 to 0.5 at tunnel speeds of 63 and 100 miles per hour.

The velocity distribution and the ramming pressure at the carburetor were obtained from measurements of total and static pressure at the flange location shown in figure 16. A grid of 29 total- and static-pressure tubes of 1/16-inch diameter was placed in the outlet to provide data for the calculations of internal drag and air quantity. The static-pressure measurements required for the determination of the critical Mach number on the upper lip (table I) of each of the inlets and at the scoop-fuselage fillets of scoop 5 were obtained by means of 1/32-inch-diameter orifices installed flush with the surfaces.

Power-on tests were made under conditions simulating high-speed and climbing flight to determine the effect of the slipstream on the available ramming pressure, the inlet velocity, and the surface pressures. At the high-speed lift coefficient of 0.1, estimated for the airplane equipped with a 1600-horsepower engine, the propeller blade angle and $V/nD$ were calculated to be 60° and 2.90, respectively. In the climb condition, for a lift coefficient of 0.5, the calculated blade angle and $V/nD$ were 40° and 1.22. The test airspeeds corresponding to the high-speed and climb conditions were 63 and 45 miles per hour, respectively.

## SYMBOLS

$\Delta C_D$   increment of drag coefficient due to scoop

$C_{D_e}$   calculated increment of drag coefficient due to external drag

$C_{D_i}$   calculated increment of drag coefficient due to internal drag

$C_L$    lift coefficient

S    wing area

$H_c$    total pressure at carbureter position

$H_o$    free-stream total pressure

p    surface pressure

q    local dynamic pressure

$q_o$    free-stream dynamic pressure

$V_1$    inlet velocity

$V_o$    free-stream velocity

Q    air quantity

$M_c$    critical Mach number

$\alpha$    angle of attack

$\beta$    propeller blade setting at 0.75 radius

D    propeller diameter

n    speed of propeller rotation

T    propeller thrust

$T_c$    thrust coefficient   $(T/\rho V_o^2 D^2)$

## RESULTS AND DISCUSSION

A typical set of tuft observations made at the entrance of scoop 3 and presented in figure 19 illustrates the importance of the inlet-velocity ratio $V_1/V_o$ as a fundamental parameter in the inlet design. The tuft observations at the low value of $V_1/V_o = 0.21$ show that the boundary layer at the center of the scoop separates from the fuselage, resulting in the formation of a thick layer of eddying flow at the bottom of the inlet which upsets the main flow into the duct. Boundary-layer separation at the inlet

occurs when the inlet static pressure $q_0 [1 - (V_1/V_0)^2]$ exceeds the total pressure of the fluid in the boundary layer approaching the inlet. The pressure at the inlet varies from stagnation pressure at an inlet-velocity ratio of zero to stream static pressure at an inlet-velocity ratio of 1.00. The dependency of boundary-layer separation on the inlet-velocity ratio is shown in figures 19(b) and 19(c) in which, for $V_1/V_0 = 0.36$, the pressure rise at the inlet was insufficient to cause large-scale separation and, for $V_1/V_0 = 0.53$, the boundary layer entered the scoop with no indication of unstable flow.

Although the inlet-velocity ratio is one of the most fundamental inlet parameters, direct comparison of the various scoops cannot be made on this basis alone. At a given $V_1/V_0$ a larger air quantity enters the larger inlets and, consequently, the duct losses, which are primarily a function of internal dynamic pressure, are higher. The parameter $Q/V_0$, in which $Q$ is the air-flow volume, provides a basis for comparison of the duct installations as a function of the air-flow quantity.

## Air Flow and Ram

Contours of total pressure (figs. 20 to 26) at the flange location are given for all the installations tested to facilitate the visualization of the air flow at the carburetor. The average value of the total pressure at the carburetor is the ramming pressure, which is given as a percentage of the free-stream dynamic pressure. Since the static pressure was uniform in most of the tests, the contours also approximately indicate the velocity distribution at the metering venturi. The ram obtained with the better scoops on airplane A was consistently lower than that obtained with similar scoops on airplane B, as a result of the higher bend losses that occurred at the abrupt duct bend on airplane A, as compared with those caused by the larger radius bend on airplane B (figs. 17 and 18).

The total-pressure distribution, which was essentially uniform for all the protruding scoops at low inlet-velocity ratios, became increasingly irregular at higher values of $V_1/V_0$. The uniformity of flow at very low-flow ratios is due to mixing in the diffuser as a result

of a turbulent condition at the inlet and to the low losses at the duct bend. At inlet-velocity ratios below about 0.30, the desirable flow uniformity is accompanied by an undesirable loss of ram owing to the flow breakdown at the duct inlet. For larger values of the inlet-velocity ratio from approximately 0.30 to 0.50, optimum over-all performance of the scoop is attained with a uniform velocity distribution at the carburetor and maximum ramming pressure.

As the flow through the carburetor system is increased with greater values of $V_1/V_0$ and $Q/V_0$, the duct bend losses become larger, tending to decrease both the flow uniformity and the available ram. At the bend the greater part of the energy losses occur on the inner side of the turn because of separation of flow around the small inner radius. This effect is shown for scoop 1 (fig. 20) at a $V_1/V_0$ value of 1.13 and a $Q/V_0$ value of 0.16. The pressure available behind the inside of the turn was about 20 percent less than at the outside of the turn, and the average ram was 78.5 percent $q_0$ as compared with 91.5 percent $q_0$ for a flow ratio of 0.05. The same effects are clearly shown in figures 21 to 24.

An analysis of the source of the loss of ram is made in figure 27, in which the pressure in the carburetor has been plotted against $V_1/V_0$ for inlets 1, 3, 4, and 5. Because of difference in inlet area, the flow quantities at the same inlet-velocity ratios for the several scoops are different.

These data all show the characteristic decrease in ram with increasing inlet-velocity ratio with the effect accentuated for the large-area inlet scoops. In the analysis of the data it was assumed that the losses in the bend were proportional to the local dynamic pressure and, based on studies of bends, it was estimated that the loss in the case of the abrupt bend in model A would be 40 percent q.

The bend losses, calculated on the foregoing assumption, are shown in figure 27. It will be noted that, for the high-flow quantity, the bend loss accounts for a large part of the total loss in ram with a smaller, more nearly constant amount caused by the boundary-layer and duct losses. At very low inlet-velocity ratios the bend losses are small and, as previously mentioned, the low ram is due to separation at the inlet. The extent of the dissymmetry occurring at the carburetor for the high flow ratios will largely de-

pend on the efficiency of the bend. The results indicate
that in high-altitude flight, for which case the duct ve-
locities may become high, extreme care must be exercised
in the design of the duct to avoid large losses in ram
and loss in flow uniformity.

The data obtained on scoops 6, 7, and 8, tested on
model B, are of particular interest in demonstrating the
effect of the inlet position with reference to the fuse-
lage surface. Scoop 6 was so located that the inlet area
was entirely above the surface with a narrow gutter pro-
vided for bypassing the boundary layer; scoop 7 was so
mounted that the local surface of the inlet was tangent to
the surface of the fuselage; and inlet 8 was flush with
the upper contour of the fuselage with no protruding
scoop. The rams obtained with scoops 6 and 7 were both
high and about the same (fig. 25). For the flush inlet 8,
only 75.5 percent $q_0$ was recovered as ram and the veloc-
ity distribution at the carburetor was very irregular.
The pressure at the inside of the turn was only about half
the stream pressure, indicating a breakaway flow ahead of
the duct inlet. In effect the external stream overruns
the inlet, that is, it fails to make an efficient turn
without the guiding action of the protruding scoop. On
the basis of ram and velocity distribution, scoops 6 and 7
are of equal merit; as will be noted later, however, the
drag of the scoop with the gutter is higher.

The effect of decreasing the height of the duct in-
let while maintaining a comparable inlet area is shown in
figure 27. At low values of $V_1/V_0$ the flat scoop has
about the same effectiveness as the scoops that protruded
farther above the surface; at high values of $V_1/V_0$, how-
ever, the ram is largely decreased. This result is attrib-
uted to the greater length of fuselage surface from which
the boundary layer is taken, resulting in a larger percent-
age of the air entering the duct at a reduced total pres-
sure. Additional factors contributing to the low rams at
high-flow quantities are the less favorable expansions in
the duct diffuser and the small hydraulic radius caused
by the flat shape with resultant increased skin friction.

The results obtained with the unconventional annular
inlet 9 are shown in figure 26. At angles of attack corre-
sponding to the high-speed condition, this inlet has char-
acteristics comparable with the best protruding scoops.
At high angles of attack, however, owing to the shielded

position of the inlet above the propeller spinner and to
the tendency of the flow to spill out of the top of the
cowling, the pressure in the scoop is greatly reduced. It
will be noted that, at angle of attack of $12^\circ$, the ram has
dropped to approximately 30 percent of the stream pres-
sure. In the case of the protruding scoop 5 (fig. 28), a
decrease of only about 5 percent in ram occurred over an
angle-of-attack range of $11^\circ$. Similar results were ob-
tained with other protruding scoops.

The effect of the slipstream on the ramming pressure
available at the carburetor is shown for scoops 1 to 5 in
figure 29. At a simulated high-speed operating condi-
tion, the slipstream increased the carburetor ram approx-
imately 5 percent $q_o$ for the five inlets tested. In the
climb condition, a slightly greater increment was measured.
The failure to recover a larger percentage of ram pressure
in the climb condition may be accounted for by inefficient
action of the lower section of the propeller cuff.

The improvement in power-on ram made by twisting the
inlet into the slipstream is shown in figure 30. In the
high-speed condition at an inlet-velocity ratio of 0.40
an increase of approximately 3 percent $q_o$ was measured.


## Drag

A summary of the drag data for the various carburetor-
air duct installations is given in table II. The incre-
ments $\Delta C_D$ in the table are the differences between meas-
ured drag coefficients of the model with and without the
carburetor-air systems and include the drag due to flow
through the outlet duct and the outlet losses. The values
of the drag increments given are therefore useful only for
comparing different scoop arrangements on the same model;
hence the values of $\Delta C_D$ for installations on model B
cannot be compared with those on model A because of
differences in the outlet duct system. The outlet for
model A was relatively efficient at low air-flow quanti-
ties; at large values of $Q/V_o$, however, the carburetor
air was ejected from the fuselage at a large angle to the
stream direction producing a turbulent region behind the
outlet with high drag. On model B, the outlet duct was
unavoidably tortuous and a large part of the kinetic en-
ergy of the air flow was lost, resulting in a high outlet
drag.

The evaluation of the internal and external components of the drag has been accomplished by calculating the energy lost in the duct and deducting this quantity from the measured $\Delta C_D$. The internal drag coefficient $C_{D_i}$, corresponding to the losses in the duct system up to the carburetor flange, is given by the expression

$$C_{D_i} = \frac{2Q}{SV_0}\left[1 - \sqrt{\frac{H_c}{H_0}}\right]$$

In a similar way the drag coefficient corresponding to the total loss between the inlet and the outlet can be calculated by replacing the term $H_c$ in the foregoing equation by the value of the total pressure at the duct outlet. The values of $C_{D_i}$ for the different carburetor installations are given in table II, in which it will be noted that the drag due to loss ahead of the carburetor is small.

The values of the drag coefficients corresponding to the total internal duct losses are not tabulated. They were calculated, however, and the external drag coefficient increment $C_{D_0}$ was obtained by deducting the total internal drag coefficient from the drag coefficient increment measured in the force test. As previously mentioned, the external drag coefficients include the losses occurring at the outlet and are therefore larger than for normal installations with engines. The results indicate, with respect to measurements at low airspeeds, that the drags of the different scoops tested are somewhat similar and that an efficient installation of a carburetor scoop on a conventional pursuit airplane should not increase the drag coefficient by more than 1 percent.

## Compressibility

As a result of numerous fundamental aerodynamic investigations, a technique has been evolved in which pressure measurements at low airspeeds are used to estimate the speed at which compressibility effects become critical. This critical speed has been defined as the forward speed at which the local velocity at any point on a body reaches the speed of sound; at speeds below the critical a well-defined variation of pressure distribution with speed occurs that is accompanied by significant drag changes. The drags of the scoops as measured in this investigation

at 100 miles por hour may bo increased considorably at
higher airplano speeds, if the local speed of sound is ap-
proached at any point on tho scoop.

The method of ostimating tho critical speed from
moasuromonts of tho prossuros at low spoods is givon in
roforonco 2. Tho valuo of tho maximum nogativo prossuro
is dotormined by moans of surfaco prossuro moasuromonts at
low spoods and this valuo is oxtrapolatod to high Mach
numbors as in figuro 31. Tho critical speed is determined
by the intersection of the extrapolated pressure curve
with the curve of the local speed of sound.

Examination of figure 31 shows that the highest crit-
ical spoods will be obtained with scoops having the low-
ost maximum nogative prossures. The problem of designing
a scoop with a high critical speed is analogous to that of
dosigning an airfoil with tho samo charactoristics bo-
causo, as in tho caso of an airfoil, tho prossuros aro do-
tormined by tho cambor of tho lip, its thicknoss, and its
anglo of attack. Tho anglo of attack at tho scoop inlot
is dotorminod by tho amount of flow that passos through and
around tho inlot which is oxprossod by tho ratio $V_1/V_0$.
At low valuos of $V_1/V_0$ the anglo of attack is high and
the converse also holds (fig. 32). Minimum negative pres-
sures would be obtained for a thin-lip scoop adjusted
throughout the flight range so as always to operate at its
ideal angle of attack. In the usual case, however, ad-
justable inlet scoops are undesirable and the optimum
scoop becomos a compromise for best average operation over
the flight range, with the specific requirement that a
critical spoed on the scoop lip must exceed that of the
rest of the airplane. The compromise involved in the de-
sign of fixed-area inlet scoops requires discarding thin
scoop lips because of their known undesirable sensitivity
to changes in angle of attack. In tho prosent investiga-
tion, sufficient thickness was provided at the scoop lips
to minimize the variation in pressure distribution with
the inlot-velocity ratio.

The prossuro distributions moasurod on tho scoops
tostod in this investigation for a rango of scoop lip
shapos and inlot-velocity ratios aro shown in figuros 33
to 41. In the analysis of tho rosults for tho difforent
scoop modifications, the minimum nogativo prossuro poaks
occur on tho contours that provido tho nost uniform pros-
suro distribution. This uniform prossuro distribution is
associatod with shapos that aro corroctly camborod for

tho anglo of attack at which thoy aro oporating. In'gon-
oral, tho poak prossures aro docroasod by incroasing tho
radius of curvaturo in tho rogion of nogativo prossuro.

Tho lowor poak prossuros accompanying tho incroasod
valuos of inlot-volocity ratio aro shown in figuros 36 to
40. In tho caso of scoop 1 with tho original contour, tho
poak nogativo prossuro is docroasod fron 0.97 $q_0$ to
-0.41 $q_0$ for a variation in tho inlot-volocity ratio fron
0.34 to 1.13. This rosult corrosponds to a chango in crit-
ical Hach numbor from 0.59 to 0.74, which is oquivalont to
an incroaso in tho critical spood fron 411 to 510 niloz
per hour at 25,000 foot altitudo. A sinilar variation of
critical spood with inlot-volocity ratio occurs for tho
othor scoops. Tho critical variation of tho prossuro dis-
tribution on tho inlot with tho inlot-volocity ratio nay
lead to the use of adjustable scoops for efficient opera-
tion over wide rangos of spood and altitude.

The effects of propeller operation on the pressure
distribution on twisted scoop 5 are shown in figures 39
and 40. Along the left fillet, the side fron which the
propeller approaches the scoop, a small decrease in the
naximum negative pressure was caused by the slipstream at
the sinulated high-spood condition (fig. 39). The pres-
sures along the top of the scoop and in tho right fillet
were not greatly affected. With the increased slipstroam
velocity sinulating tho clinb condition (fig. 40), a fur-
thor roduction of tho negativo pressures in the left fil-
let occurrod accompaniod by slight roductions in the poak
prossuros on tho top and on tho right fillot. For tho
tosts with tho inlot-volcity ratio of about 1.00, tho
peak nogativo prossuros occurrod on tho insido lip of tho
scoop duo to tho nogativo anglo at which tho lip was op-
orating.

CONCLUSIONS

Fron tho rosults obtainod for oight scoops tostod in
tho full-scalo tunnol, it has boon concludod:

1. Tho inportant dosign paranotors that dotornino
tho oporational charactoristics of carburotor-air scoops
aro tho inlot-volocity ratio $V_1/V_0$ and tho air-flow
quantity $Q/V_0$.

2. Flow separation occurs in the boundary layer ahead of the carburetor inlet if the inlet-velocity ratio is decreased below about 0.30.

3. Highest over-all inlet efficiencies occur for values of $V_1/V_0$ between 0.40 and 0.50.

4. One of the most important sources of loss of ram and nonuniformity of flow at the carburetor is the duct bend. The velocity at the duct bend should be reduced to as low a magnitude as feasible.

5. Raised carburetor scoops with gutters for bypassing the boundary layer show no important increases in ram over well-designed scoops that are tangent to the fuselage. The drag of the raised scoop is higher.

6. Lower ram and less uniform velocity distribution were obtained with wide flat scoops at high inlet-velocity ratios.

7. The drag of a well-designed carburetor air scoop should not exceed 1 percent of the airplane drag.

8. The minimum negative pressure peaks and highest critical speed are obtained on scoop contours that provide a uniform pressure distribution. Highest critical speeds are reached at high inlet-velocity ratios.

9. The critical variation of the pressure distribution on the inlet with $V_1/V_0$ may lead to the use of adjustable scoops for efficient operation over wide ranges of speed and altitude.


Langley Memorial Aeronautical Laboratory,
    National Advisory Committee for Aeronautics,
        Langley Field, Va.


## REFERENCES

1. DeFranco, Smith J.: The N.A.C.A. Full-Scale Wind Tunnel. Rep. No. 459, NACA, 1933.

2. von Kármán, Th.: Compressibility Effects in Aerodynamics. Jour. Aero. Sci., vol. 8, no. 9, July 1941, pp. 337-356.

**TABLE I.**

**SCOOP LIP**

**SECTIONS**

All dimensions
are in inches



y

→ x
(parallel
to ship
center
line)

θ

Tube 1

| Station | Upper surface, y | | | | | | | | | | |
|---|---|---|---|---|---|---|---|---|---|---|---|
| x | Scoop 1 | | | | Scoop 3 | | | Scoop 4 | | Scoop 5 | | |
| | Orig. | A | B | C | Orig. | A | B | Orig. | A | West | C.L. | East |
| 0 | 0.72 | 0.74 | 0.62 | 0.64 | 0.77 | 0.69 | 0.59 | 0.57 | 0.54 | 1.00 | 0.83 | 1.82 |
| .25 | .92 | .97 | .92 | .89 | .99 | .97 | .95 | .76 | .80 | —— | 1.00 | —— |
| .50 | 1.09 | 1.15 | 1.15 | 1.25 | 1.15 | 1.20 | 1.20 | .93 | 1.00 | 1.29 | 1.15 | 2.22 |
| .75 | 1.24 | 1.31 | 1.34 | 1.45 | 1.32 | 1.39 | 1.40 | 1.10 | 1.17 | —— | 1.27 | —— |
| 1.00 | 1.38 | 1.44 | 1.48 | 1.52 | 1.46 | 1.54 | 1.57 | 1.24 | 1.31 | 1.48 | 1.37 | 2.56 |
| 1.25 | 1.50 | 1.58 | 1.63 | 1.67 | 1.58 | 1.69 | 1.73 | 1.37 | 1.44 | —— | 1.49 | —— |
| 1.50 | 1.62 | 1.70 | 1.74 | 1.80 | 1.70 | 1.81 | 1.89 | 1.52 | 1.59 | 1.61 | 1.59 | 2.88 |
| 1.75 | 1.72 | 1.81 | 1.86 | 1.92 | 1.80 | 1.91 | 1.99 | 1.62 | 1.69 | —— | 1.67 | —— |
| 2.00 | 1.84 | 1.91 | 1.96 | 2.00 | 1.89 | 2.02 | 2.10 | 1.73 | 1.80 | 1.69 | 1.75 | 3.15 |
| 2.50 | 2.00 | 2.09 | 2.15 | 2.20 | 2.05 | 2.17 | 2.25 | 1.91 | 1.98 | 1.73 | 1.89 | 3.43 |
| 3.00 | 2.14 | 2.23 | 2.30 | 2.44 | 2.17 | 2.31 | 2.39 | 2.04 | 2.11 | 1.76 | 2.00 | 3.72 |
| 3.50 | 2.27 | 2.37 | 2.43 | 2.49 | 2.27 | 2.41 | 2.49 | 2.17 | 2.24 | 1.78 | 2.11 | 3.95 |
| 4.00 | 2.40 | 2.50 | 2.55 | 2.61 | 2.35 | 2.50 | 2.58 | 2.28 | 2.35 | 1.80 | 2.19 | 4.22 |
| 4.50 | 2.50 | .. | | | 2.42 | 2.57 | 2.65 | 2.38 | 2.45 | 1.80 | 2.26 | 4.46 |
| 5.00 | 2.58 | | | | 2.47 | 2.63 | 2.71 | 2.47 | 2.54 | 1.77 | 2.33 | 4.70 |
| 5.50 | 2.65 | | | | 2.52 | 2.67 | 2.75 | 2.55 | 2.62 | 1.75 | 2.38 | —— |
| 6.00 | 2.74 | | | | 2.56 | 2.71 | 2.79 | 2.68 | 2.61 | 1.73 | 2.43 | 5.13 |
| 7.00 | 2.87 | | | | 2.63 | 2.79 | 2.87 | 2.75 | 2.82 | | 2.52 | |
| 8.00 | 2.98 | | | | | | | | | | 2.60 | |
| 9.00 | 3.06 | | | | | | | | | | 2.66 | |
| R | .45 | .40 | .32 | .22 | .45 | .32 | .23 | .38 | .30 | .68 | .57 | 1.06 |
| $x_1$[a] | | .09 | .15 | .22 | | .14 | .22 | | .07 | | | |
| $y_1$[a] | | | .05 | .08 | | .07 | .09 | | | | | |
| θ, deg. | 28 | 30 | 28 | 29 | 25 | 24 | 30 | 7 | 8 | 6 | 5 | 0 |

[a] $x_1$ and $y_1$ = ordinates of center of leading-edge radius of modified
inlets with respect to center of original lip.
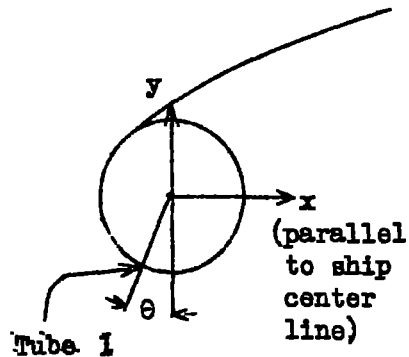
## TABLE II

### SUMMARY OF DRAG DATA

| Scoop | Inlet-area (sq in.) | $V_1/V_0$ | $Q/V_0$ | $\Delta C_D$ at $C_L=0.1$ Test speed (mph) 63 | 100 | $C_{D_1}$ | $C_{D_e}$ at $C_L=0.1$ Test speed (mph) 63 | 100 |
|---|---|---|---|---|---|---|---|---|
| 1 | 19.8 | 0.49 | 0.067 | 0.0004 | 0.0002 | 0.00004 | 0.0004 | 0.0002 |
| 2 | 30.3 | .32 | .067 | .0001 | .0002 | .00004 | .0001 | .0002 |
| 3 | 47.3 | .21 | .069 | .0003 | ----- | .00007 | .0002 | ----- |
|  |  | .31 | .102 | .0004 | ----- | .00008 | .0003 | ----- |
|  |  | .33 | .108 | .0005 | .0006 | ------ | .0004 | .0005 |
|  |  | .36 | .118 | .0003 | ----- | .00008 | .0002 | ----- |
|  |  | .43 | .141 | .0003 | ----- | .00011 | .0001 | ----- |
|  |  | .50 | .164 | .0007 | ----- | .00016 | .0004 | ----- |
|  |  | .53 | .174 | .0010 | ----- | .00019 | .0006 | ----- |
| 4 | 32.7 | .27 | .061 | ----- | .0003 | .00005 | ----- | .0003 |
| 5 | 26.3 | .37 | .068 | .0003 | .0003 | .00003 | .0003 | .0003 |
|  |  | .54 | .099 | .0003 | .0003 | .00005 | .0003 | .0002 |
| 6 | 37.1 | .26 | .067 | ----- | .0008 | .00001 | ----- | ----- |
|  |  | .34 | .083 | ----- | .0007 | .00001 | ----- | ----- |
|  |  | .45 | .116 | ----- | .0008 | .00003 | ----- | ----- |
| 7 | 26.9 | --- | ---- | ----- | ----- | ------ | ----- | ----- |
|  |  | .37 | .068 | ----- | .0001 | .00001 | ----- | ----- |
|  |  | .55 | .103 | ----- | .0003 | .00001 | ----- | ----- |
|  |  | .66 | .123 | ----- | .0005 | .00002 | ----- | ----- |
| 8 | 27.8 | .42 | .081 | ----- | .0002 | .00014 | ----- | ----- |
|  |  | .52 | .100 | ----- | .0005 | .00019 | ----- | ----- |
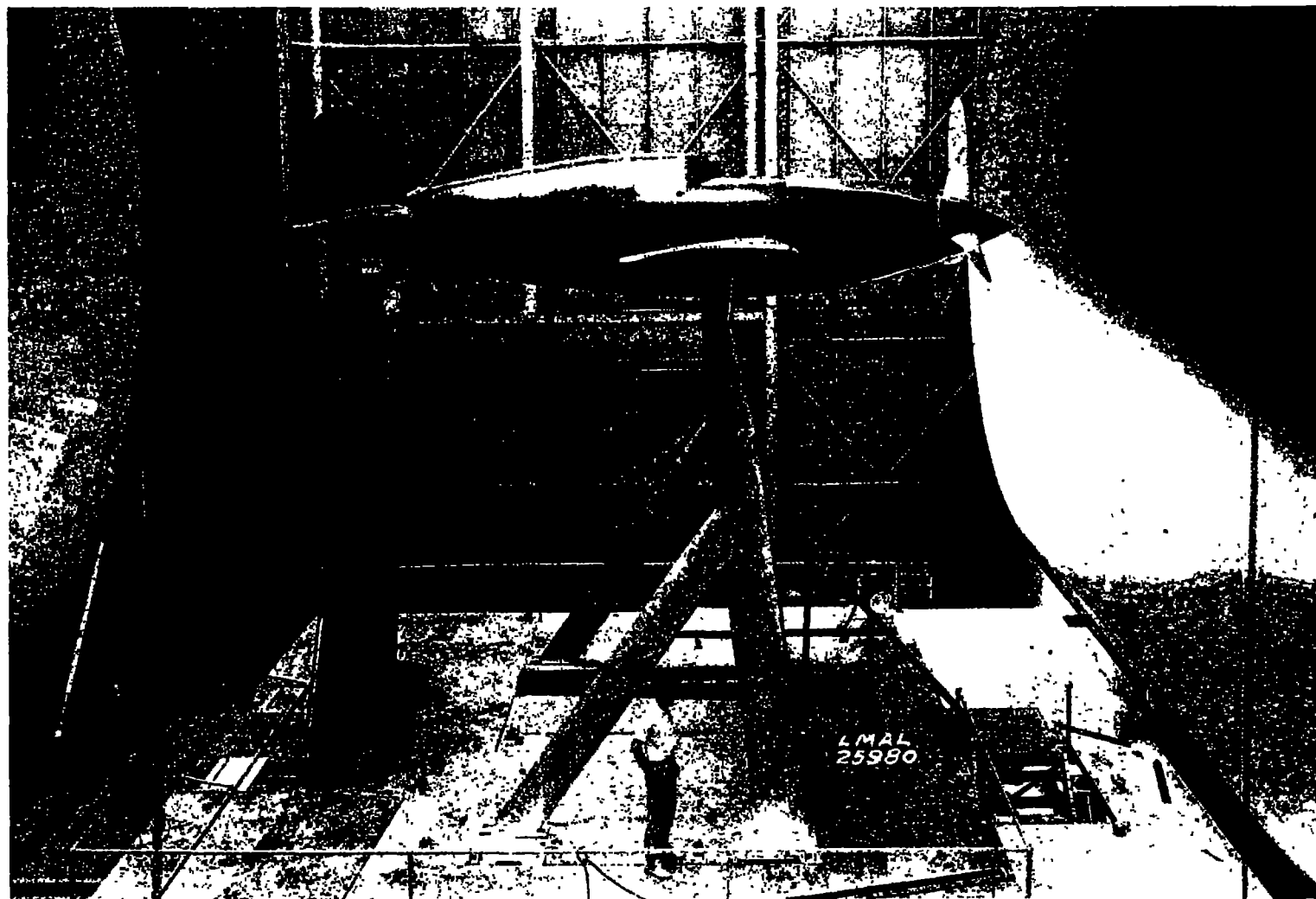
Figure 1.- Model A with carburetor air scoop 1, as tested in the full-scale wind tunnel.

Fig. 1

Fig. 2
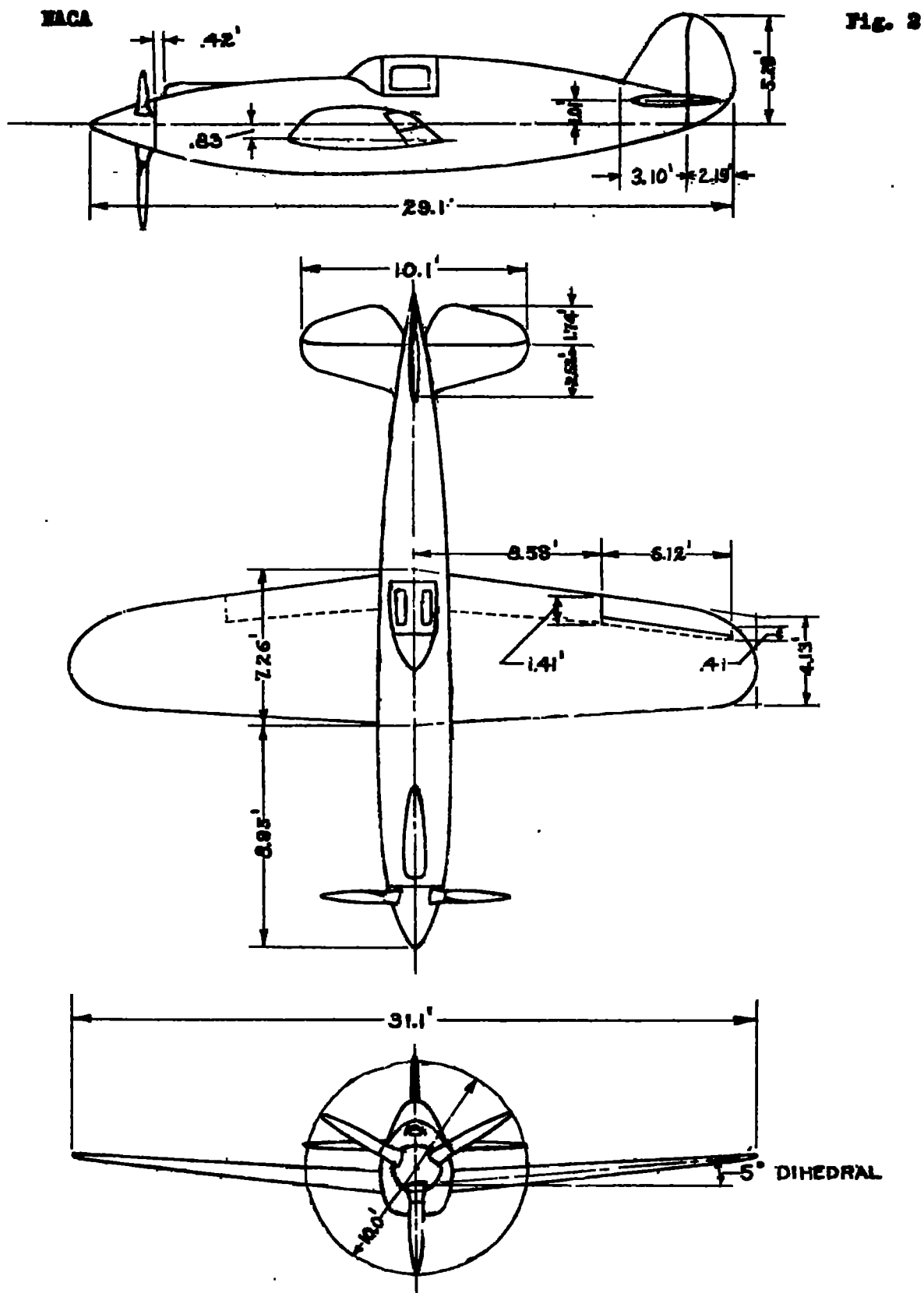


Figure 2.- General arrangement of model A.
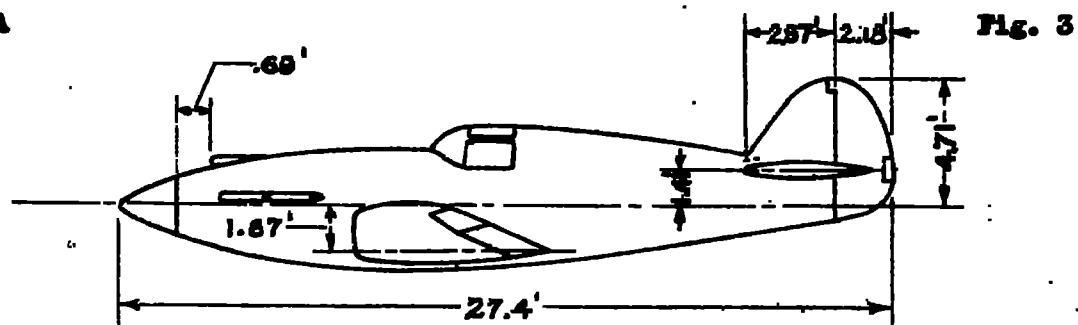
Fig. 3
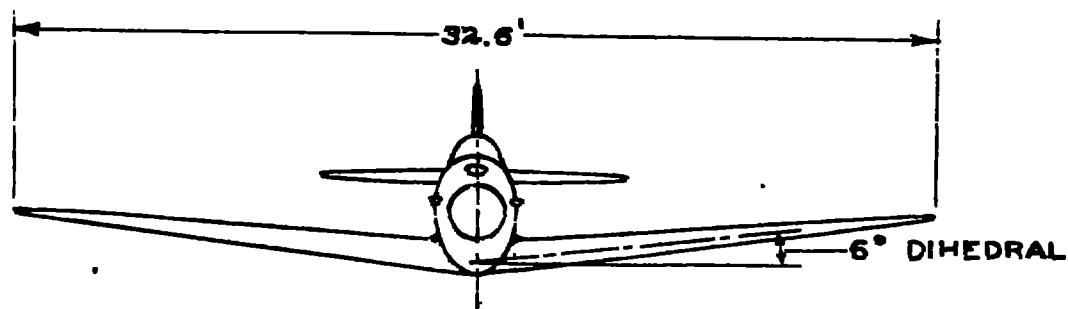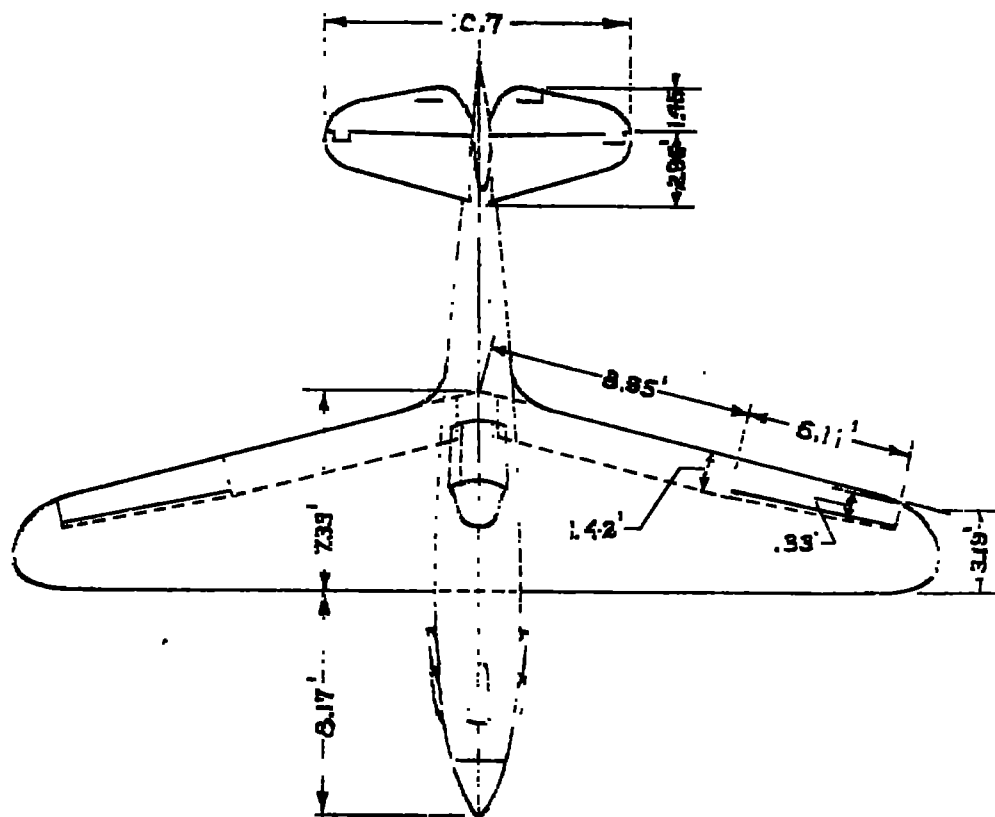
Figure 3.— General arrangement of model B.

## Section A

| $x$ | $y_U$ | $y_L$ |
|---|---|---|
| 0 | 0 | 0 |
| 0.116 | 0.280 | 0.250 |
| .232 | .390 | .315 |
| .463 | .535 | .405 |
| .694 | .645 | .465 |
| .925 | .745 | .510 |
| 1.487 | .890 | .565 |
| 1.850 | .990 | .595 |
| 2.315 | 1.065 | .600 |
| 2.775 | 1.110 | .595 |
| 3.700 | 1.135 | .575 |
| 4.625 | 1.095 | .540 |
| 5.560 | 1.000 | .465 |
| 6.475 | .840 | .385 |
| 7.410 | .625 | .280 |
| 8.330 | .360 | .165 |
| 9.250 | 0 | 0 |

$R_{L.E.} = 0.335$

$R_{T.E.} = 0.058$

## Section B

| $x$ | $y_U = y_L$ |
|---|---|
| 0 | 0 |
| 0.194 | 0.430 |
| .388 | .625 |
| .775 | .930 |
| 1.163 | 1.160 |
| 1.550 | 1.340 |
| 2.330 | 1.635 |
| 3.100 | 1.845 |
| 3.880 | 2.000 |
| 4.650 | 2.110 |
| 6.200 | 2.190 |
| 7.750 | 2.100 |
| 9.300 | 1.840 |
| 10.850 | 1.465 |
| 12.400 | 1.025 |
| 13.950 | .535 |
| 15.500 | 0 |

$R_{L.E.} = 0.520$

$R_{T.E.} = 0$
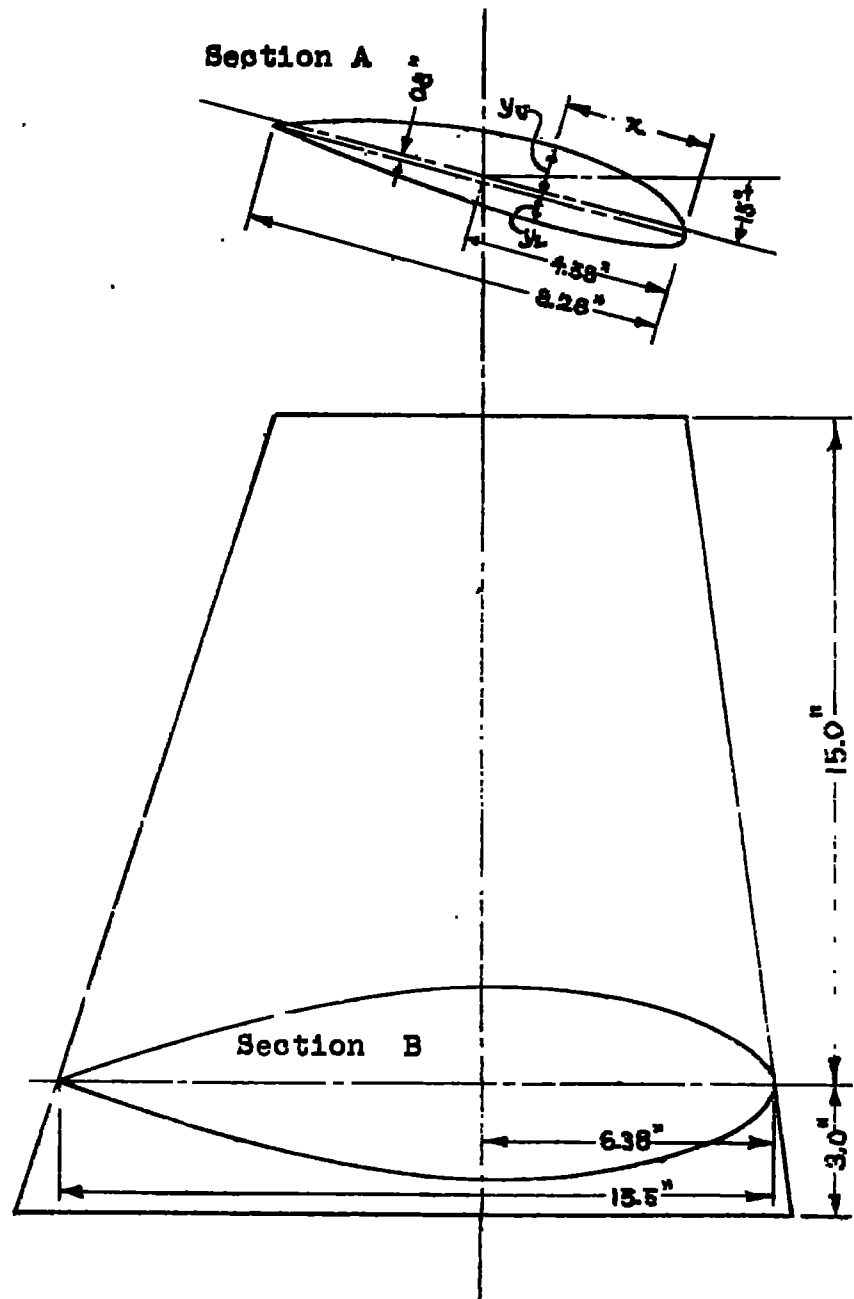


Figure 4.- Dimensions of propeller cuff.
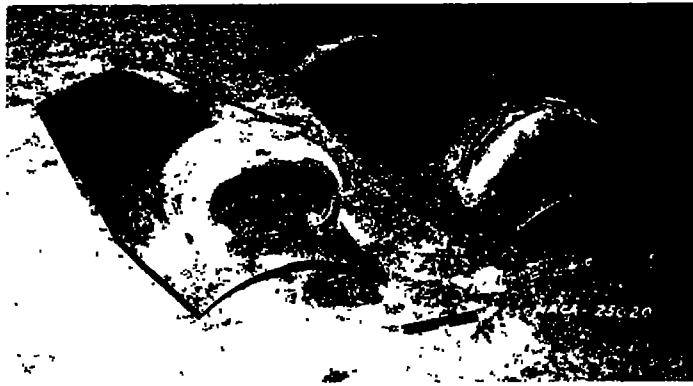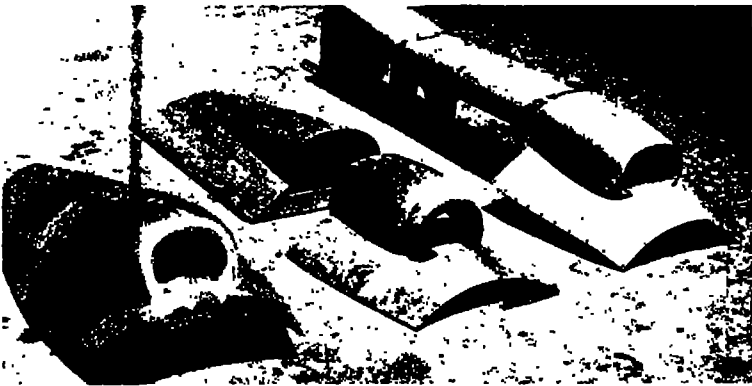
Figure 5.- Carburetor air scoops tested on model A.

Fig. 5
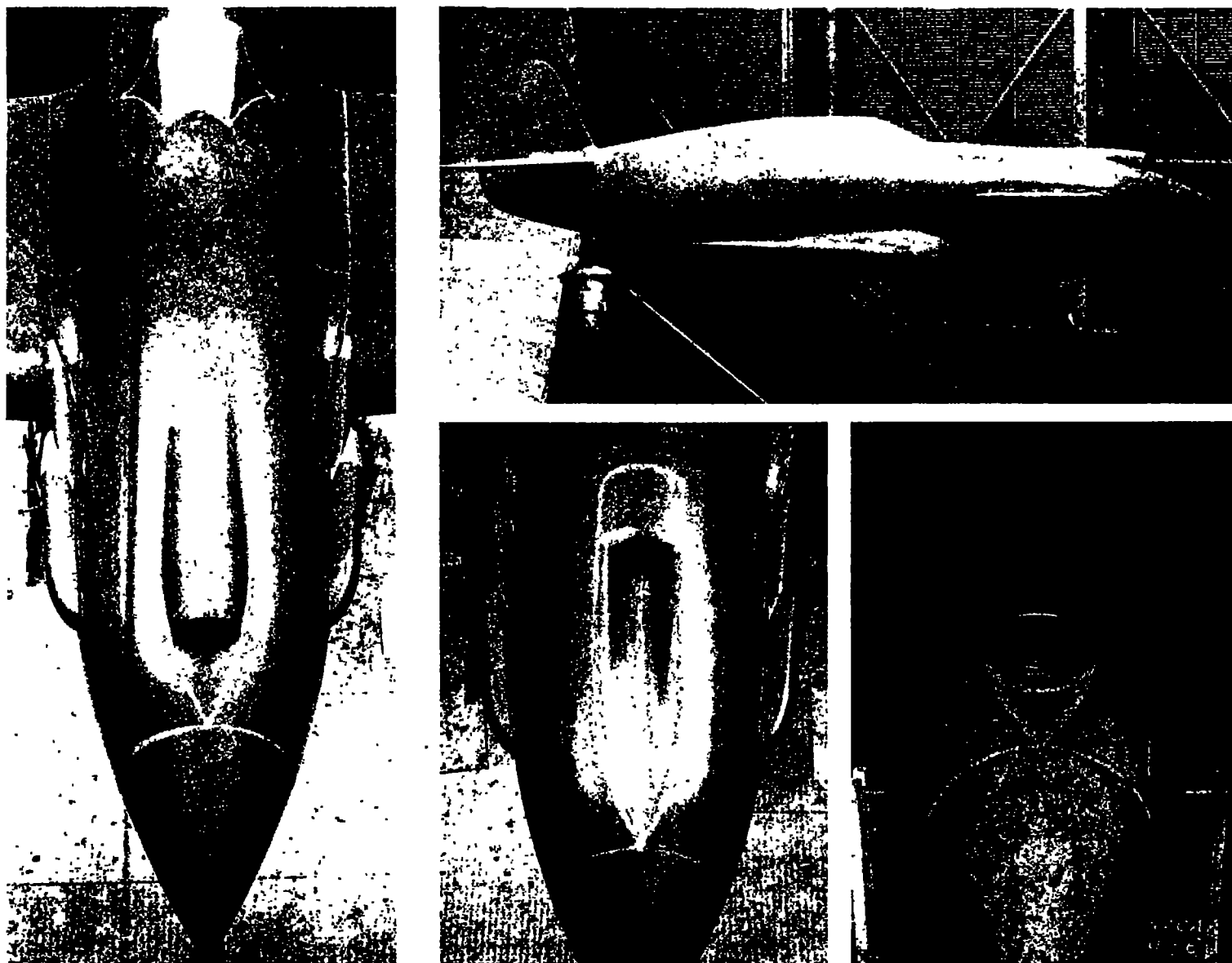
Figure 6.- Model B and scoops 6, 7, and 8.

Fig. 6

A = 19.8 SQ IN.

A = 37.5 SQ IN.

SECTION A-A

SECTION B-B
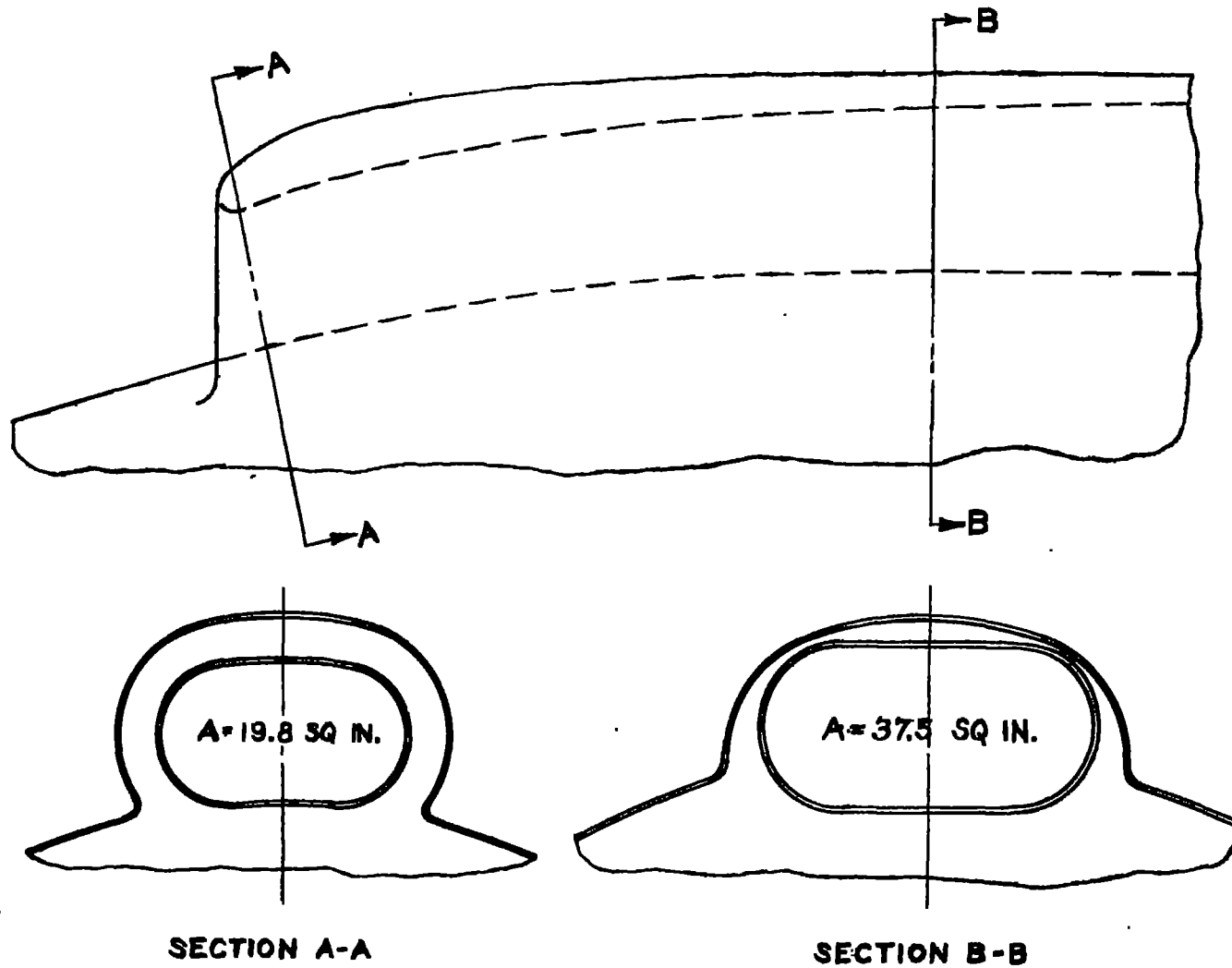
Figure 7.- Carburetor air scoop 1, tested on model A.

Fig. 7

A=30.3 SQ IN.

A = 37.5 SQ IN.

SECTION A-A

SECTION B-B
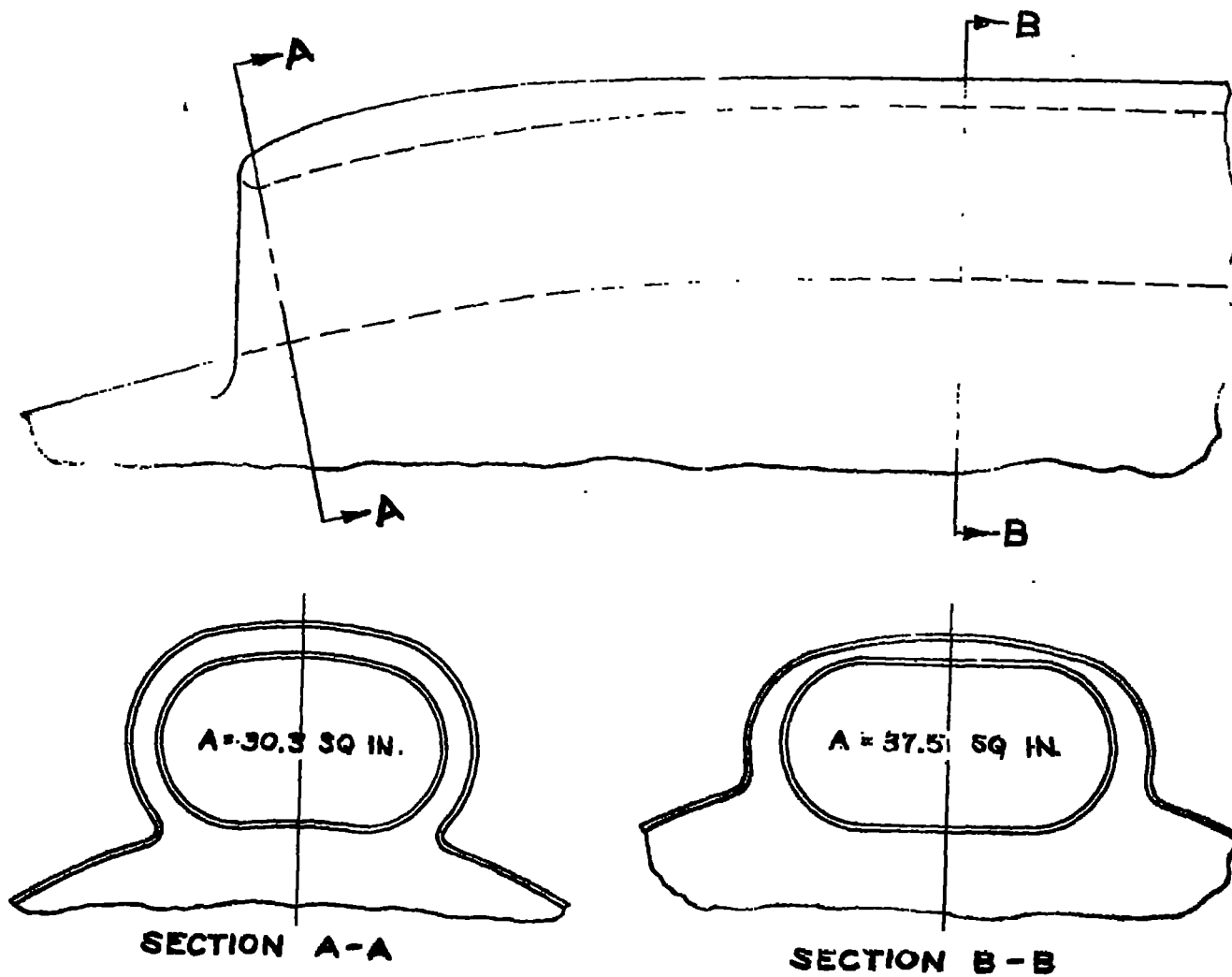
Figure 6.- Carburetor air scoop 2, tested on model A.

FIG. 6.

SECTION A-A          SECTION B-B
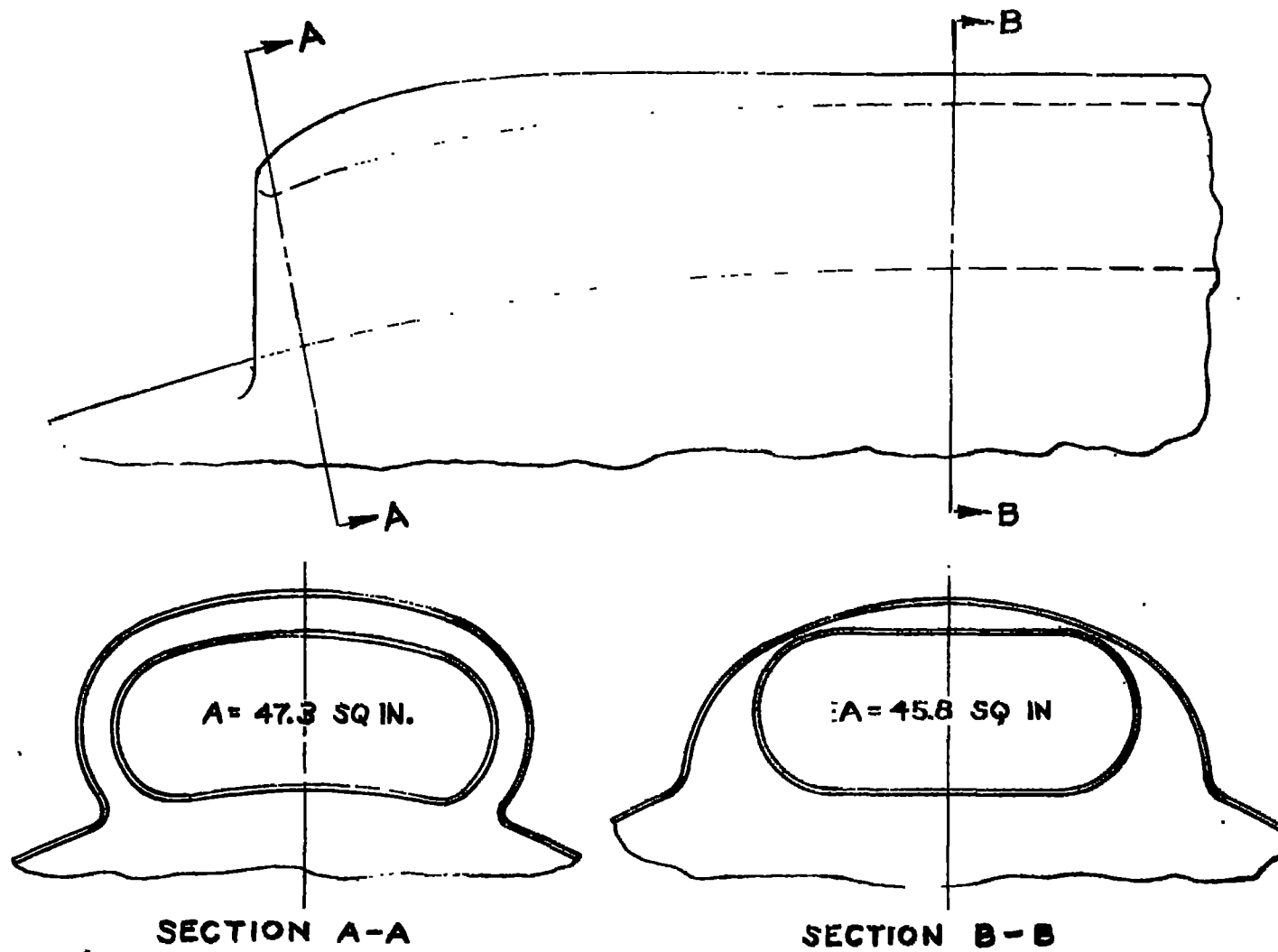
Figure 9.- Carburetor air scoop 3, tested on model A.

Fig. 9

A = 32.7 SQ IN.

A = 40.9 SQ IN.

SECTION A-A
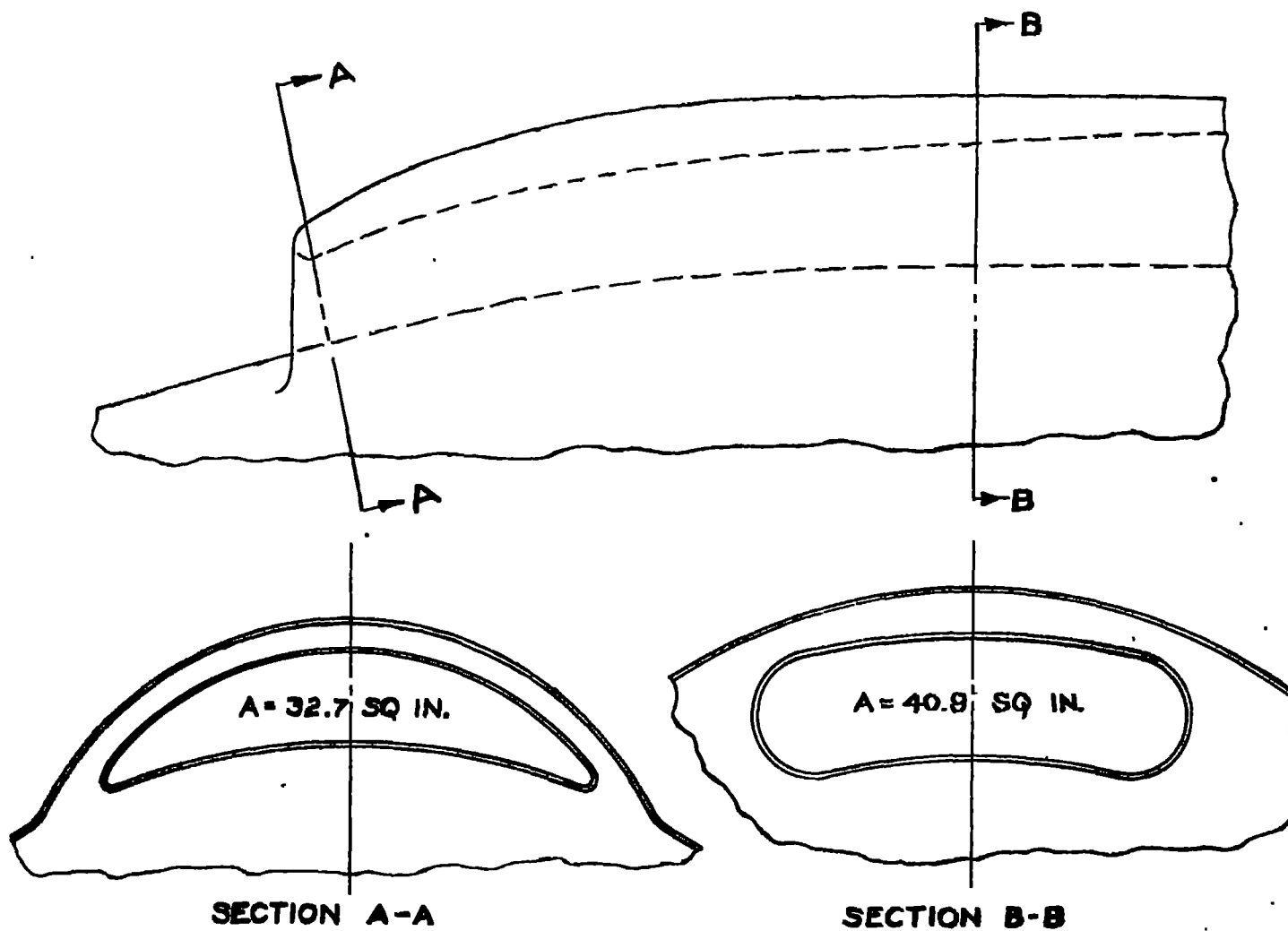
SECTION B-B

Figure 10.- Carburetor air scoop 4, tested on model A.

Fig. 10

80°

TOP VIEW

A=26.3 SQ IN.

SECTION THROUGH INLET

→ B

A=37.5 SQ IN.

SECTION THROUGH B
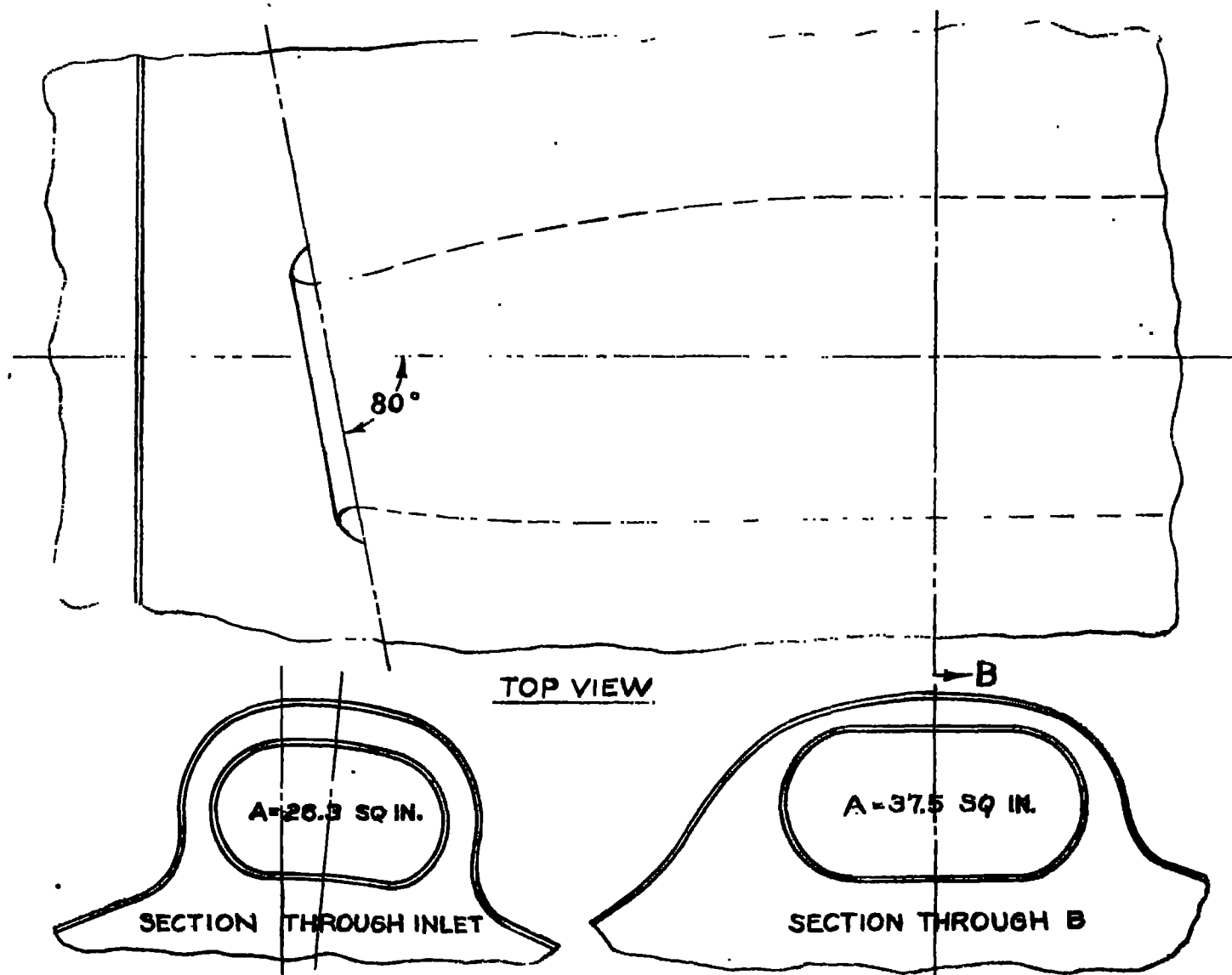
Figure 11.- Carburetor air scoop 5, tested on model A.

Fig. 11

END OF SPINNER

$6\frac{3}{4}$"

A = 37.1 SQ IN.

SECTION A-A

A = 42.5 SQ IN.

SECTION B-B

Fig. 12
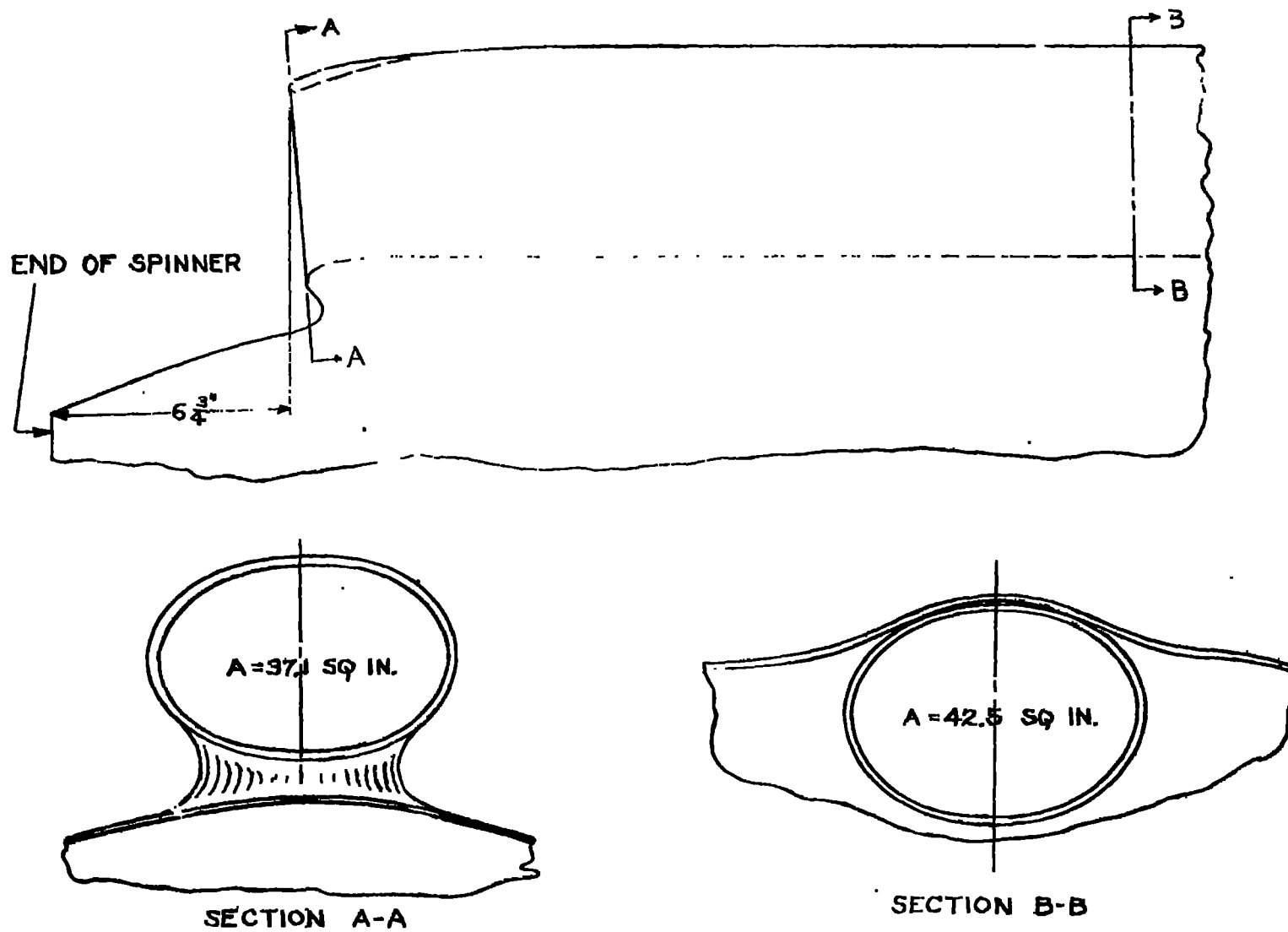
Figure 12.- Carburetor air scoop 6, tested on model B.

END OF SPINNER

A

,-A

B

B

$8\frac{1}{4}"$

A=25.9 SQ 'N.

A = 42.5 SQ IN

SECTION A-A
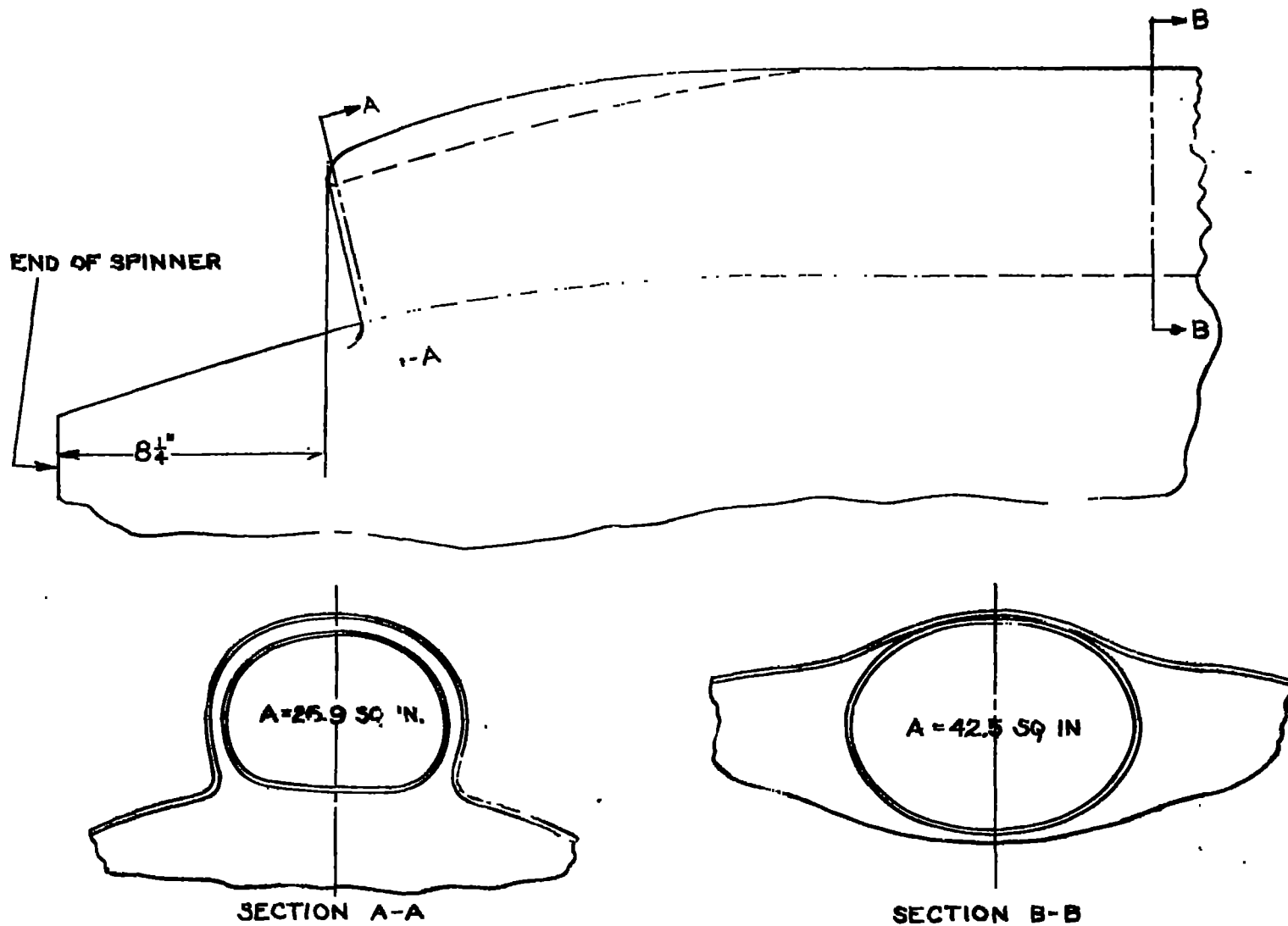
SECTION B-B

Figure 13.- Carburetor air scoop 7, tested on model B.

Fig. 13

SPINNER

$42\frac{1}{2}^{"}$

A=27.8 SQ. IN.
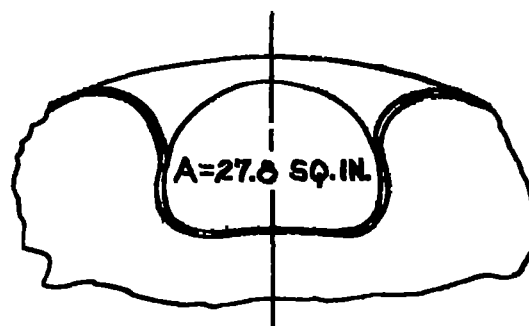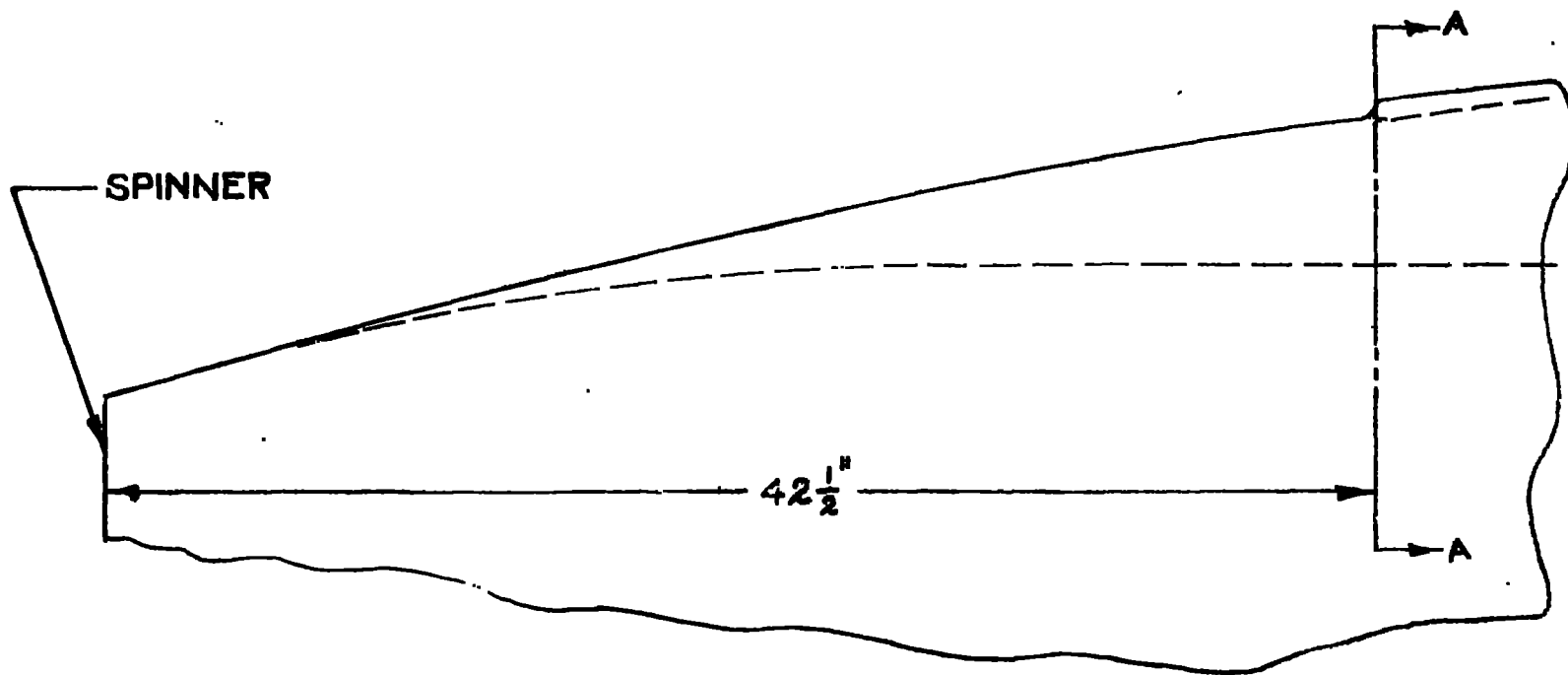
SECTION A-A

Figure 14.- Carburetor air scoop 8, tested on model B.

Fig. 14

A

A

A= 31.7 SQ IN.
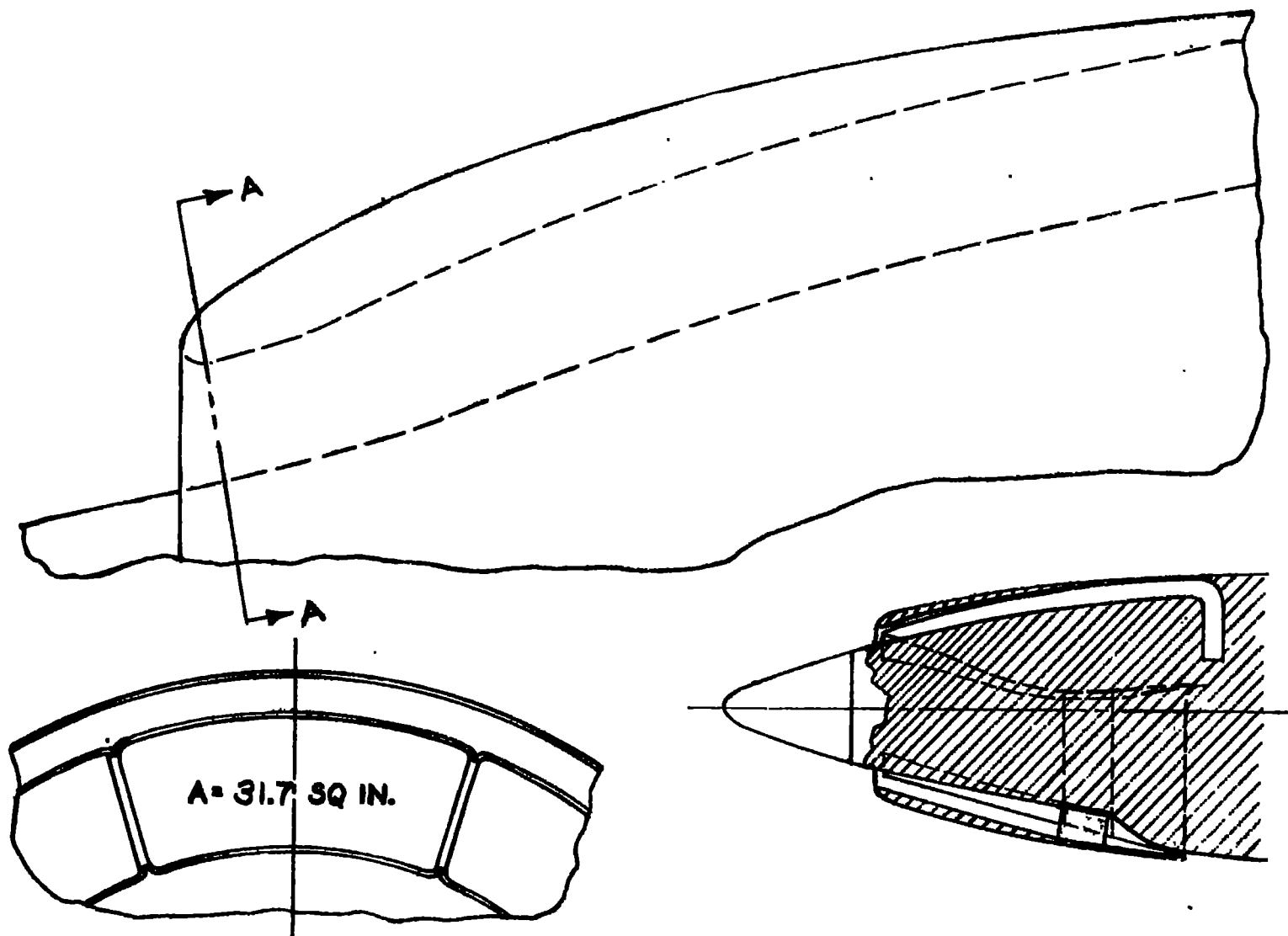
SECTION A - A

Figure 15.- Carburetor air scoop 9, tested on model A.

Fig. 15

SLIP
JOINT

CARBURETOR
FLANGE

OUTLET

INLET

$3\frac{3}{4}$R

GUIDE
VANES
(CHORD - 4")

$1\frac{1}{4}$R

$2\frac{1}{2}$R
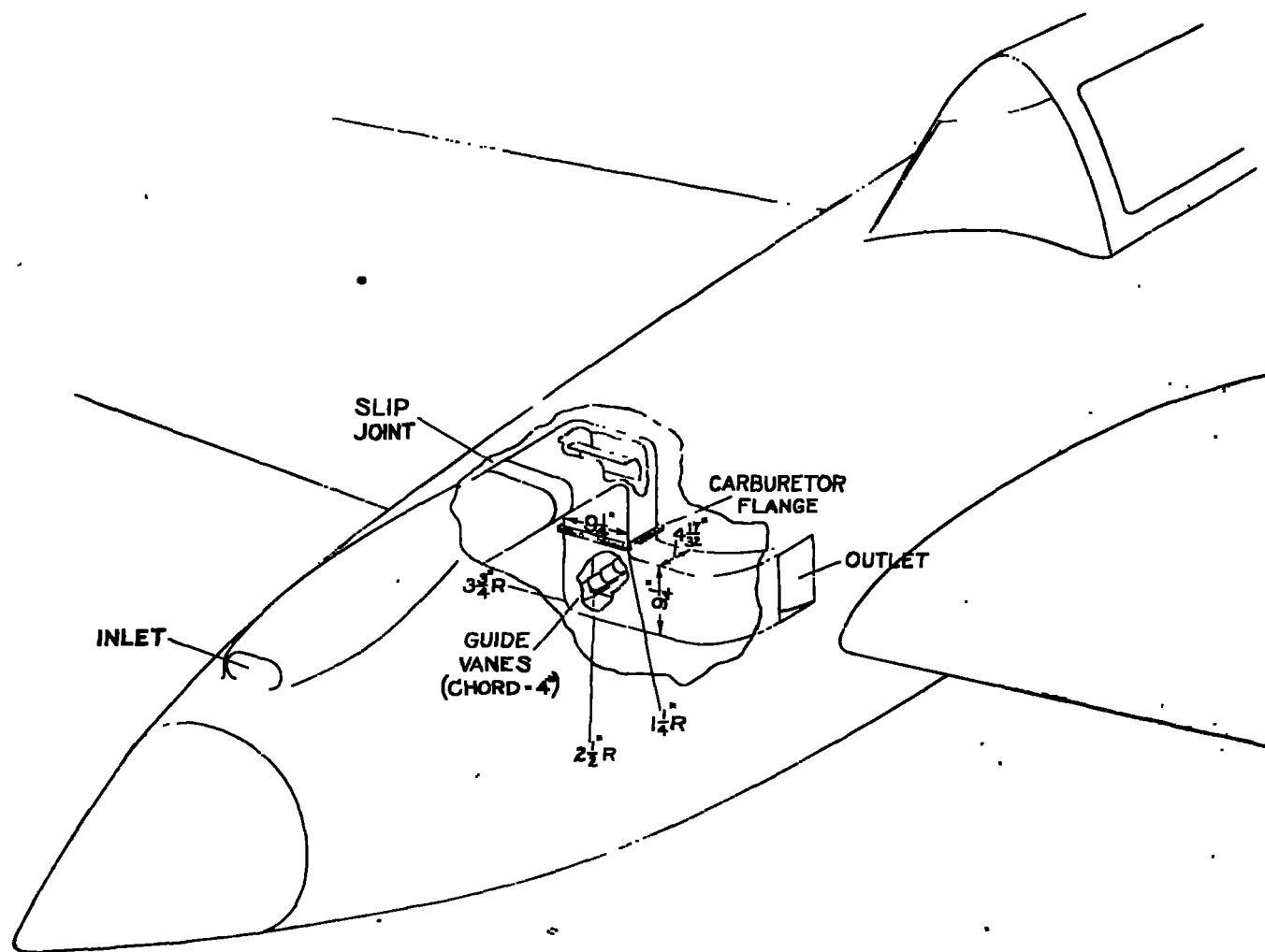
**FIGURE 16 — TYPICAL CARBURETOR AIR-SCOOP INSTALLATION
ON MODEL A.**

Fig 16
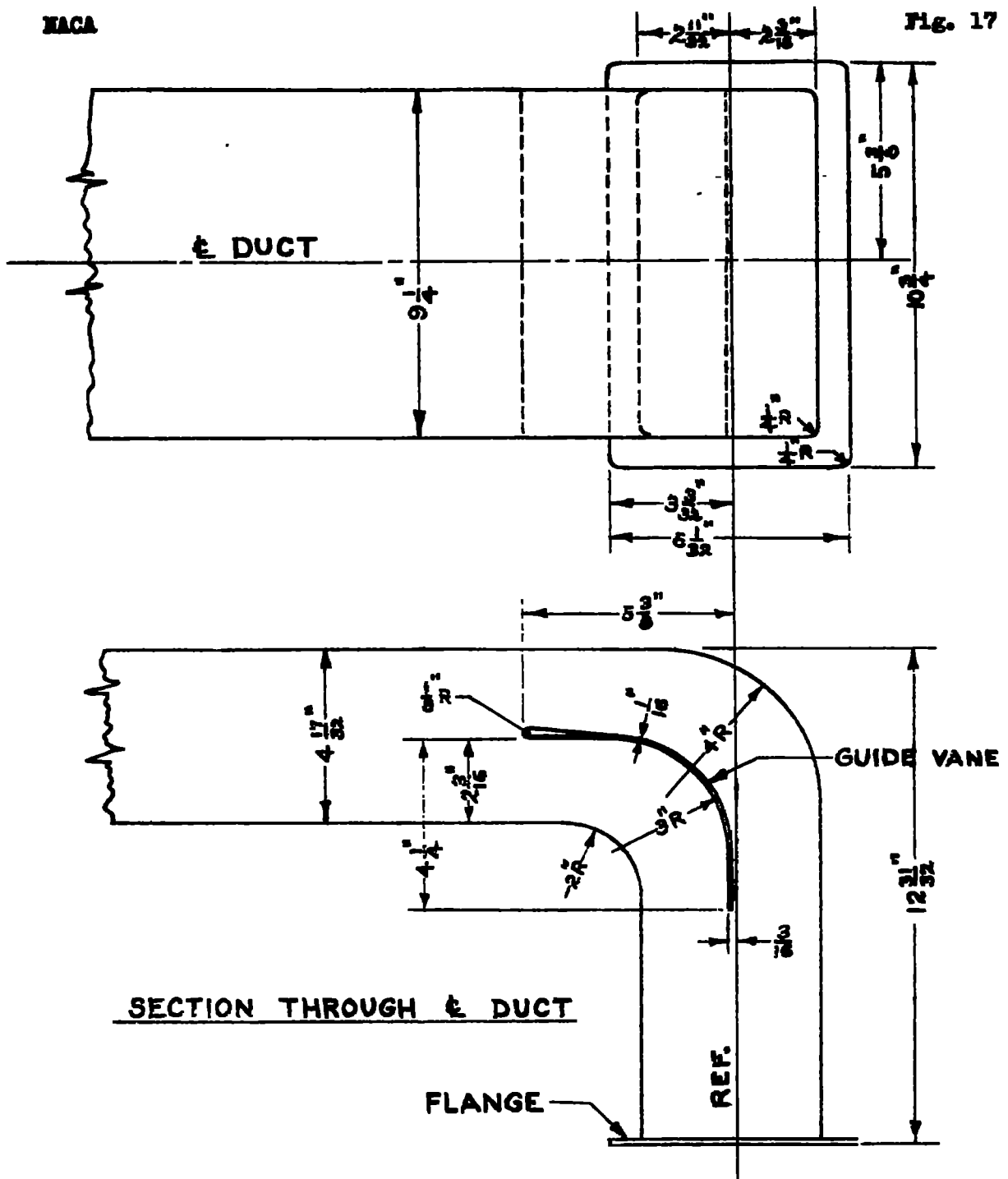
Figure 17.- Dimensions of duct turn ahead of carburetor location on model A.

Fig. 18



ELLIPTICAL

CARBURETOR FLANGE
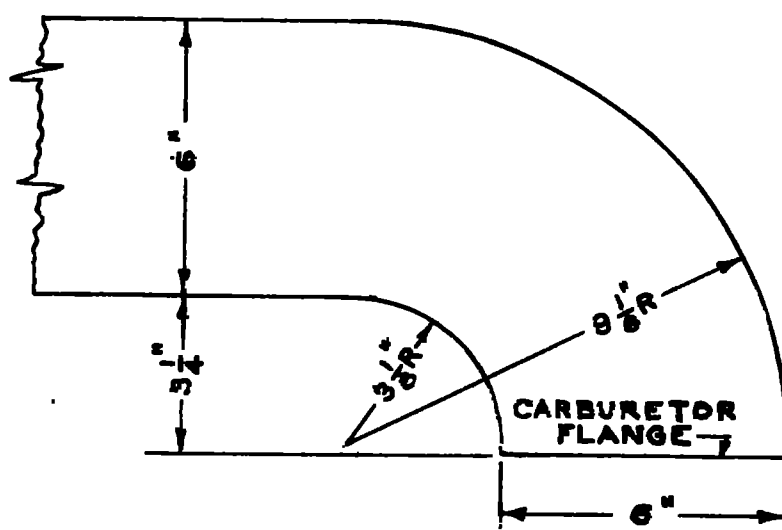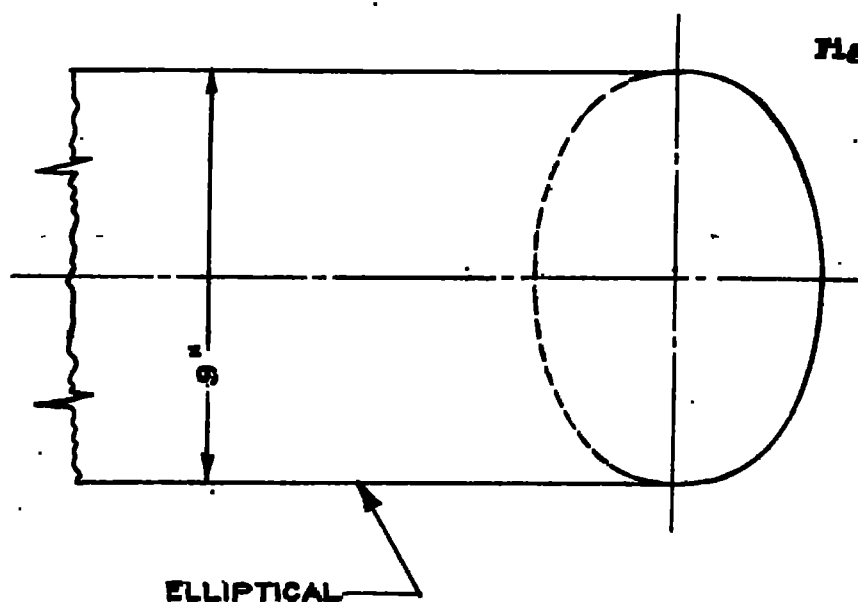
Figure 18.- Dimensions of duct turn ahead of carburetor location
        on model B.

Fig. 19



(a) $\bar{V}_1/V_0 = 0.21.$

(b) $V_1/V_0 = 0.36.$

(c) $V_1/V_0 = 0.53.$
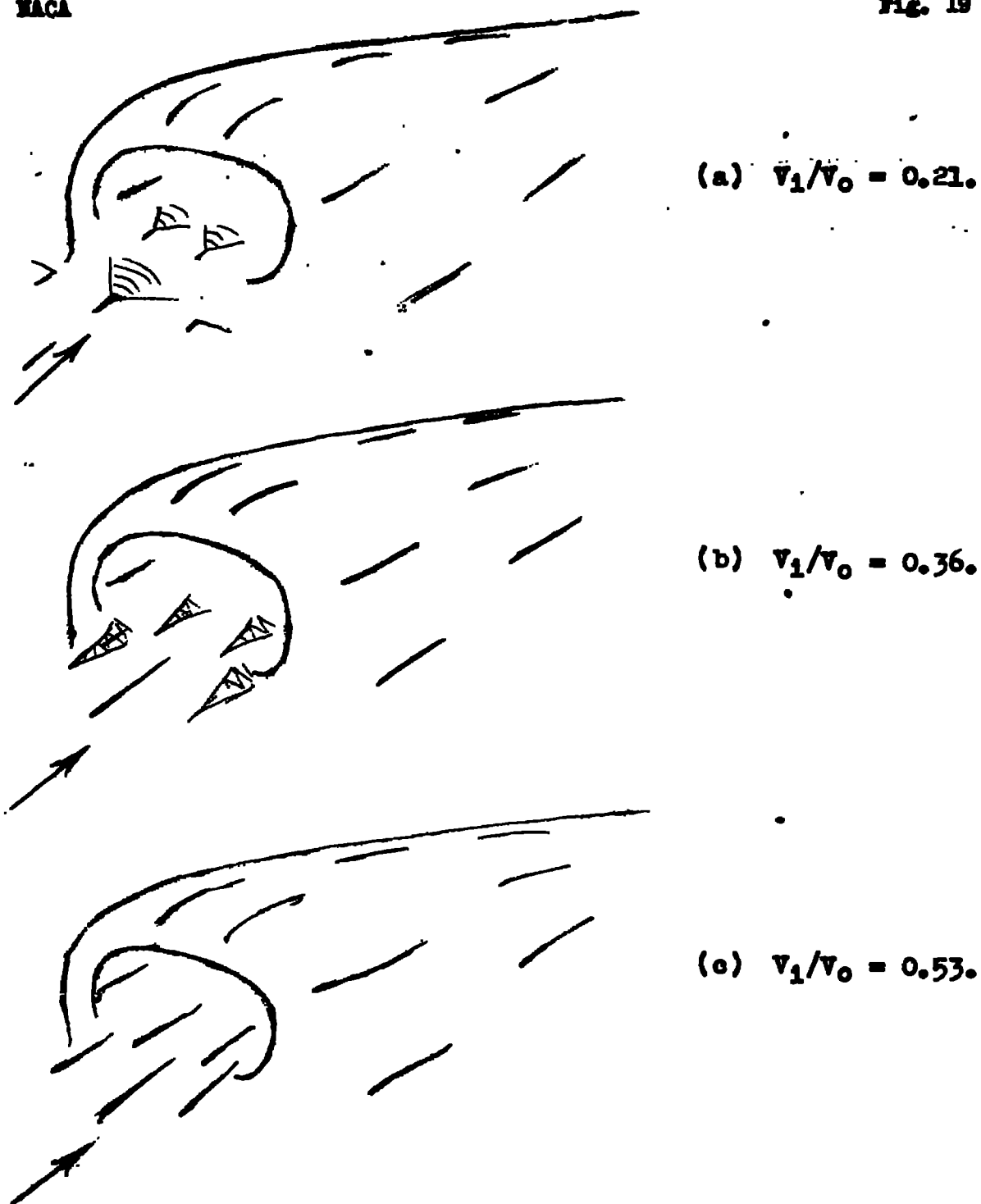
Figure 19.- Tuft survey showing effect of inlet velocity on flow
at inlet of scoop 3; propeller off.
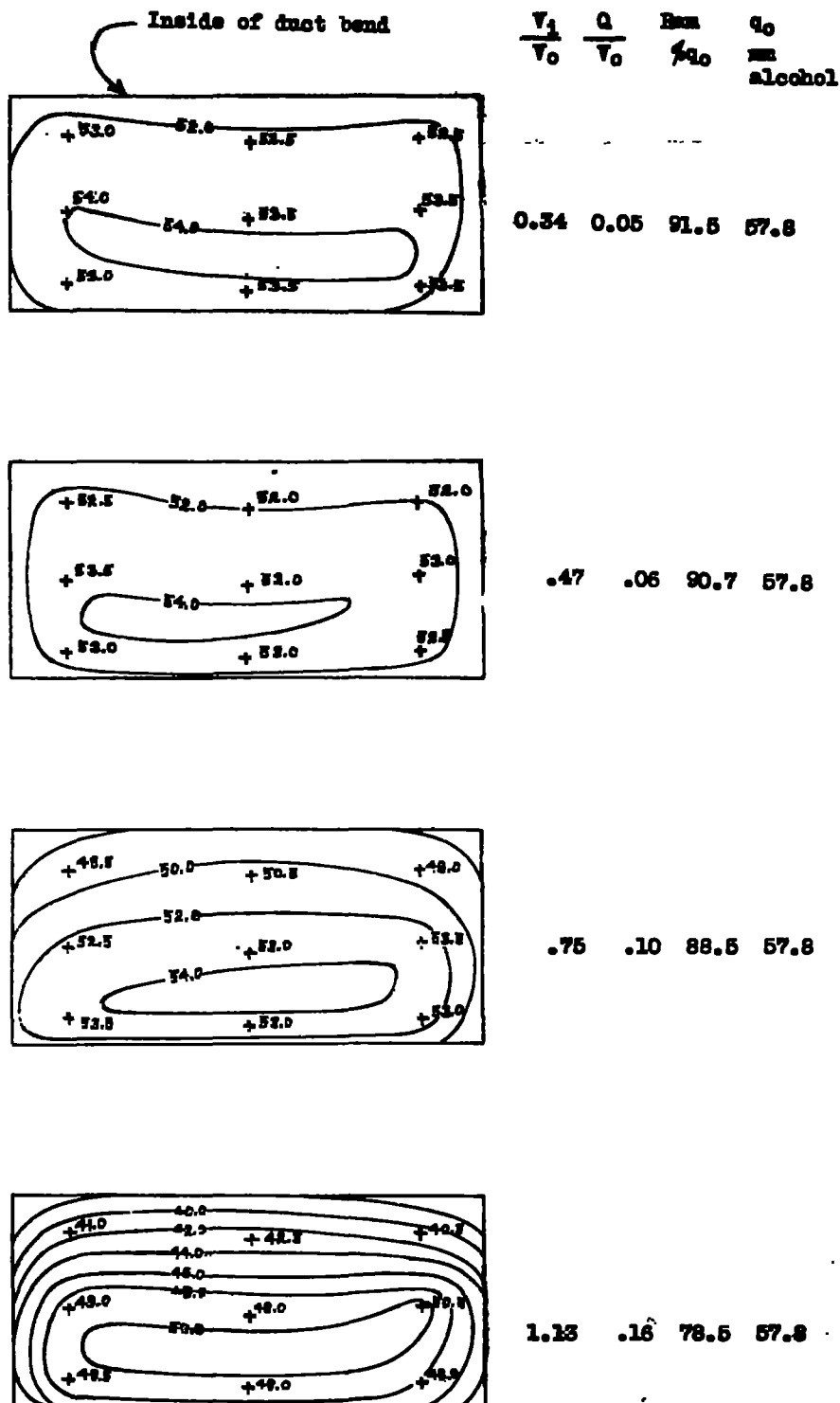
Figure 20.- Effect of $V_1/V_0$ on ram with scoop 1; propeller off, $\alpha = 1^\circ$.
Values indicate total pressure, $H_c$, in millimeters of alcohol.

Inside of duct bend

+ 54.0        + 54.0        + 54.0

+ 55.0        + 55.0        + 55.0

+ 54.0        + 54.5        + 54.5
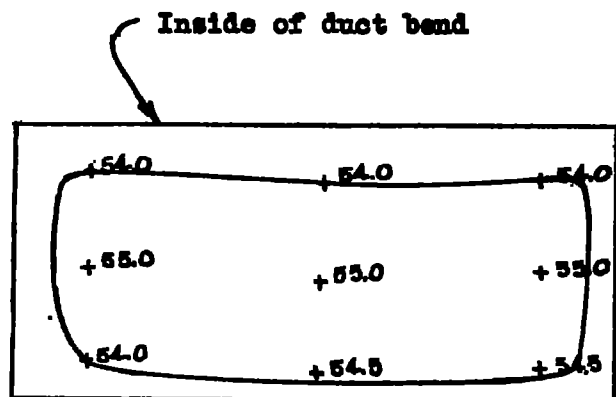
$V_1/V_0$ = 0.32    Ram = 90.8%$q_0$

$Q/V_0$ = 0.07    $q_0$ = 59.4 mm alcohol

+ 54.0        + 55.5        + 54.5

+ 56.0        + 57.0        + 57.5

+ 56.0        + 57.0        + 56.5
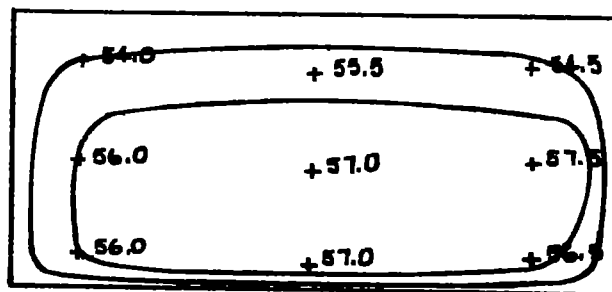
$V_1/V_0$ = 0.45    Ram = 91.6%$q_0$

$Q/V_0$ = 0.09    $q_0$ = 60.4 mm alcohol

Figure 21.- Effect of $V_1/V_0$ on ram with scoop 2; propeller off,
α = 1°. Values indicate total pressure, $H_c$, in mil-
limeters of alcohol.

Inside of duct bend
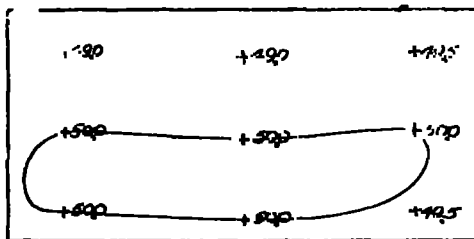
$V_1/V_0 = 0.21$   Ram = 83.7%$q_0$

$Q/V_0$ = 0.07   $q_0$ = 58.6 mm alcohol
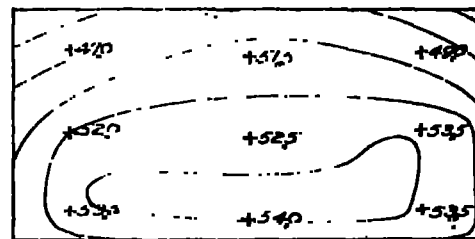
$V_1/V_0 = 0.43$   Ram = 87.5%$q_0$

$Q/V_0$ = 0.14   $q_0$ = 58.4 mm alcohol.
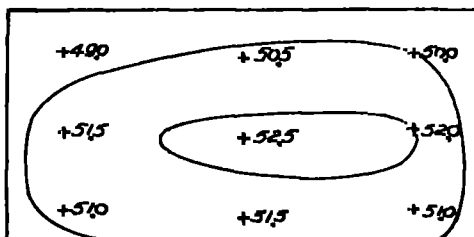
$V_1/V_0 = 0.31$   Ram = 86.7%$q_0$

$Q/V_0$ = 0.10   $q_0$ = 58.0 mm alcohol
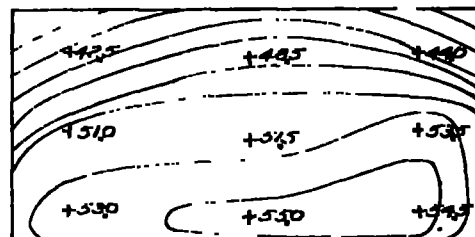
$V_1/V_0 = 0.50$   Ram = 84.3%$q_0$

$Q/V_0$ = 0.17   $q_0$ = 57.8 mm alcohol
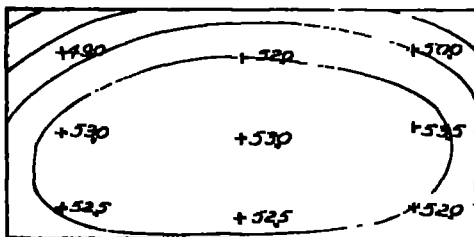
$V_1/V_0 = 0.37$   Ram = 88.2%

$Q/V_0$ = 0.12   $q_0$ = 58.2 mm alcohol
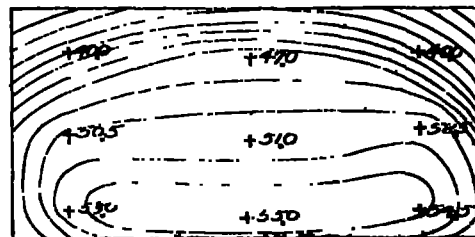
$V_1/V_0 = 0.53$   Ram = 82.2%$q_0$

$Q/V_0$ = 0.17   $q_0$ = 57.8 mm alcohol

Figure 22.- Effect of $V_1/V_0$ on ram with scoop 3; propeller off, $\alpha = 1^0$. Values indicate total pressure, $H_0$, in millimeters of alcohol.
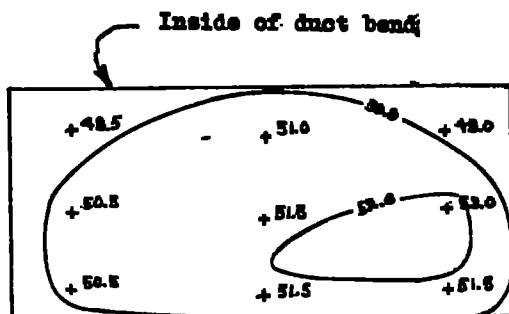
Fig. 22
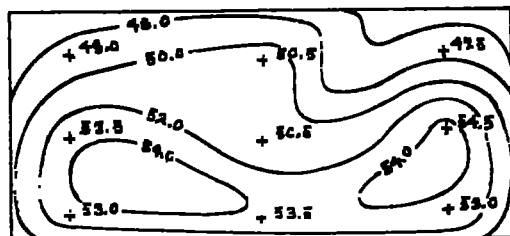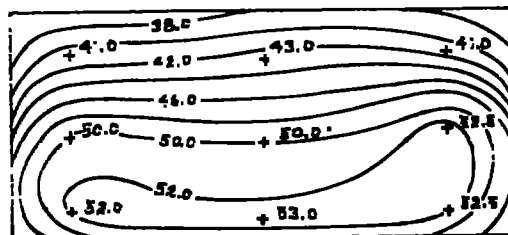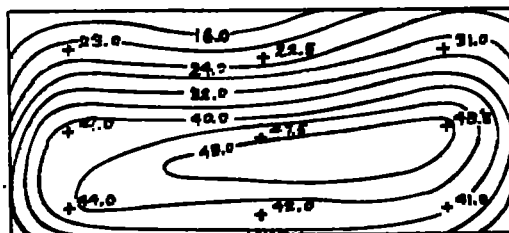
Fig. 23



Figure 23.- Effect of $V_1/V_0$ on ram with scoop 4; propeller off, $\alpha = 1°$.
Values indicate total pressure, $H_c$, in millimeters of alcohol.
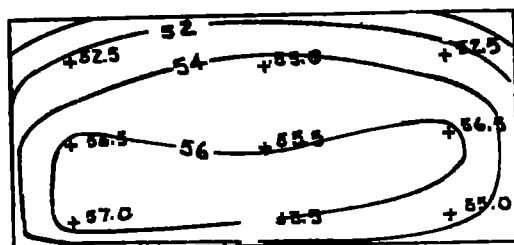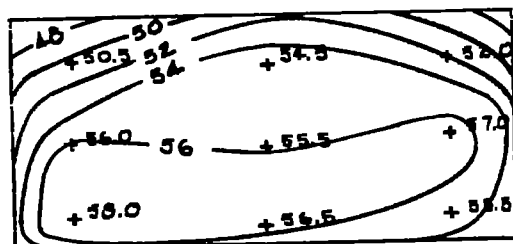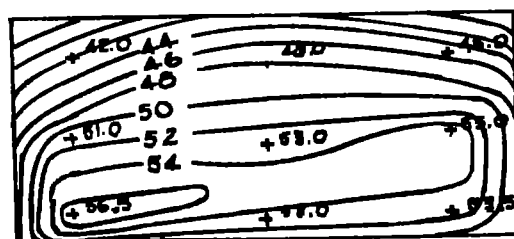
Figure 24.- Effect of $V_1/V_0$ on ram with scoop 5, propeller off, $\alpha = 1^0$.
Values indicate total pressure, $H_c$, in millimeters of alcohol.
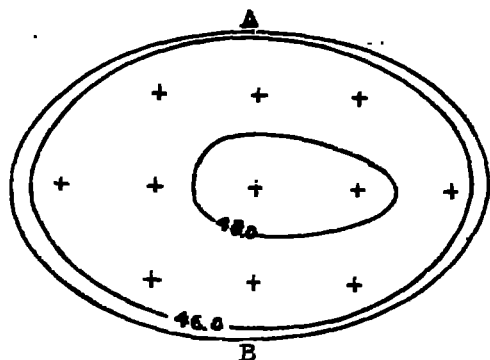
(a) Scoop 6.
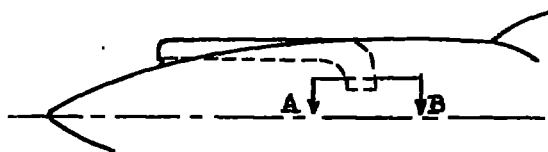
$$V_1/V_0 = 0.40 \quad \text{Ram} = 96.0\% q_0$$
$$Q/V_0 = 0.10 \quad q_0 = 49.0 \text{ mm alcohol}$$
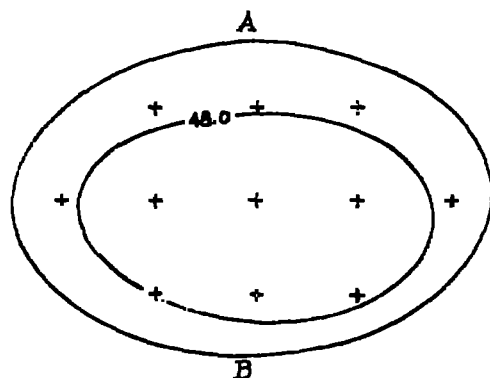
(b) Scoop 7.
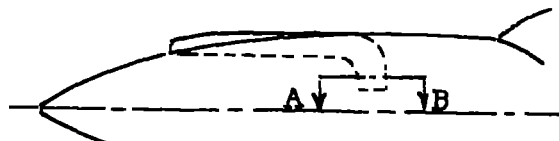
$$V_1/V_0 = 0.40 \quad \text{Ram} = 98.0\% q_0$$
$$Q/V_0 = 0.08 \quad q_0 = 48.6 \text{ mm alcohol}$$
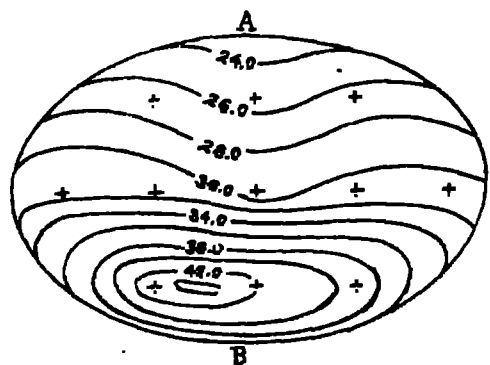
(c) Scoop 8.
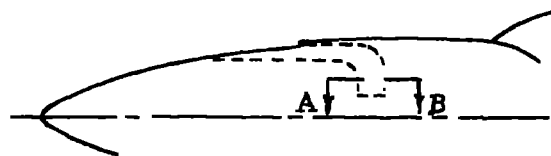
$$V_1/V_0 = 0.40 \quad \text{Ram} = 73.5\% q_0$$
$$Q/V_0 = 0.08 \quad q_0 = 49.0 \text{ mm alcohol}$$

Figure 25.- Effect of inlet position on ram.  Contour values indicate total pressure, $H_c$, in millimeters of alcohol;  propeller off, $\alpha = 1^0$.
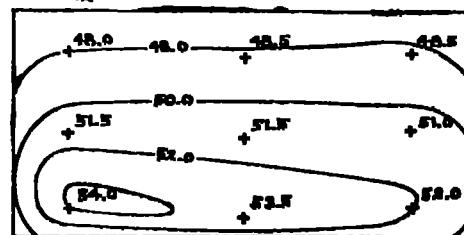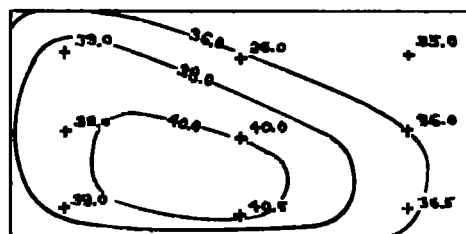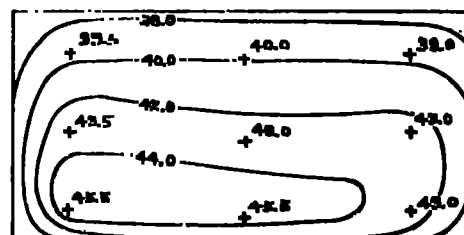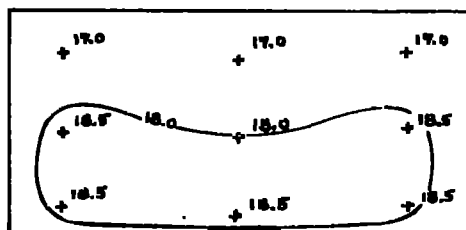
Figure 26.- Distribution of total pressure, $H_c$, with scoop 9; propeller off. Values of $H_c$ are in millimeters of alcohol.
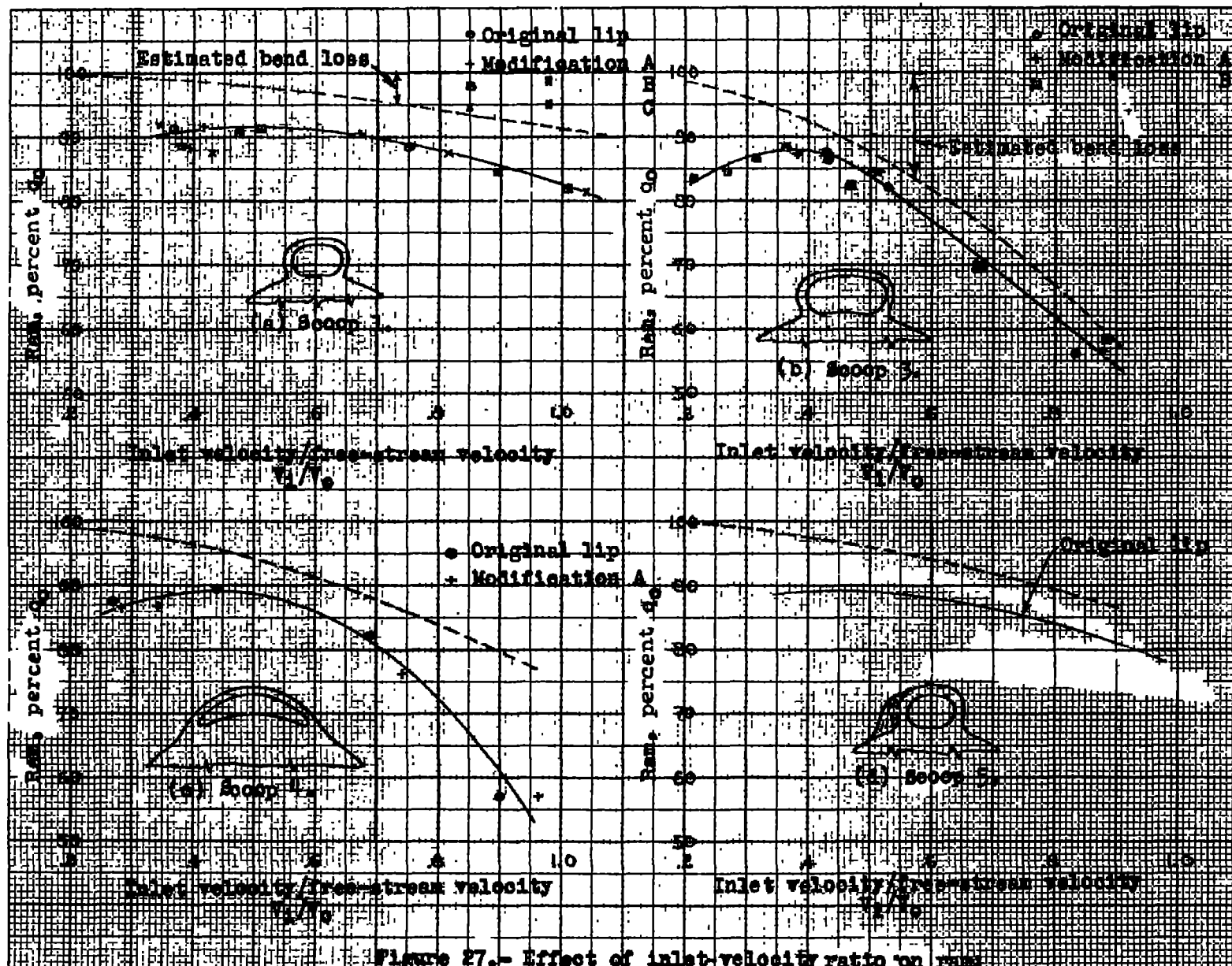
Figure 27.- Effect of inlet-velocity ratio on ram; propeller off, α = 1°.
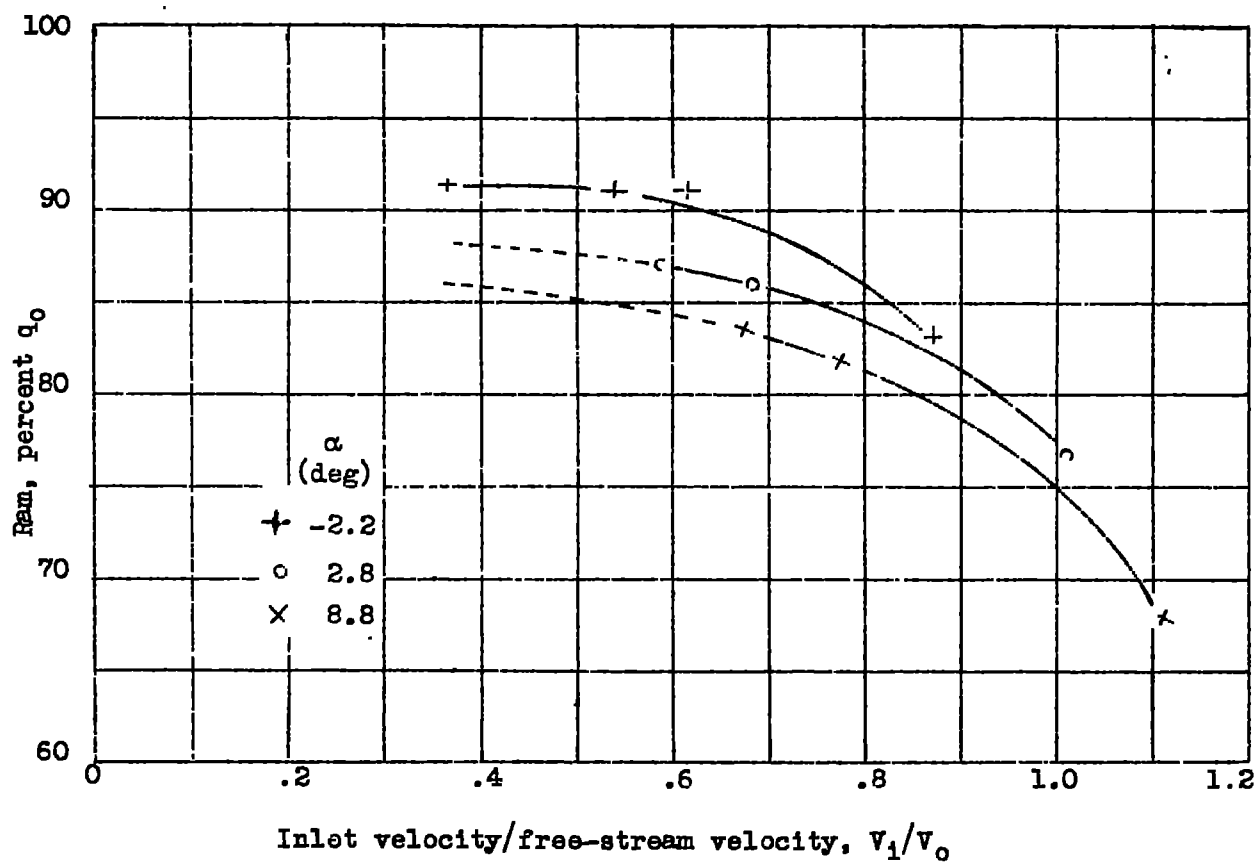
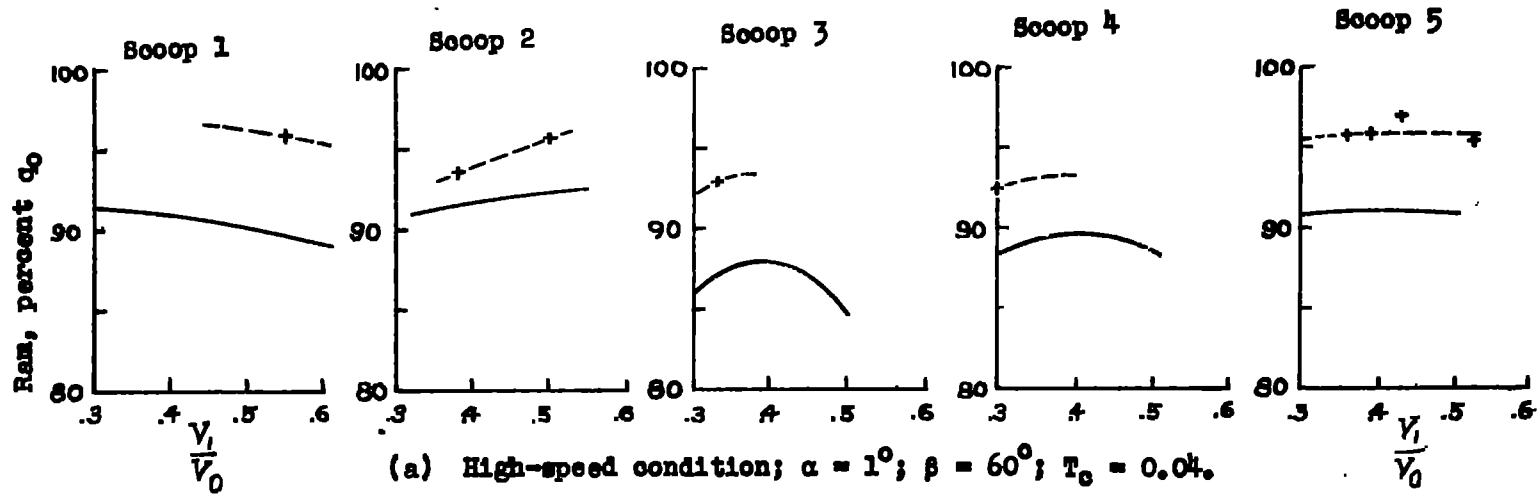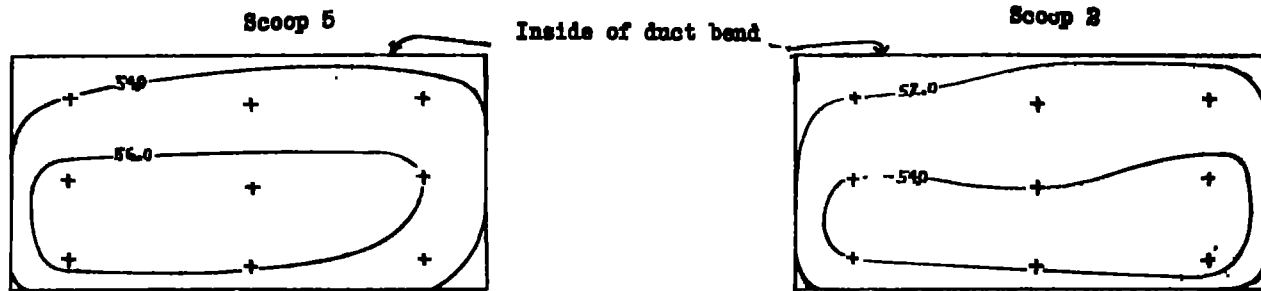Figure 28.– Effect of angle of attack on ram; scoop 5, propeller off.

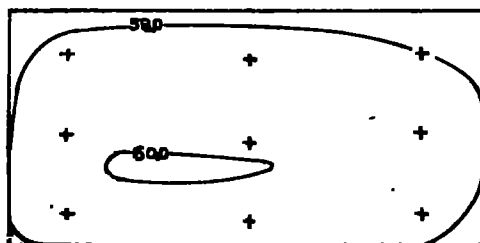(a)  High-speed condition; $\alpha = 1^{\circ}$; $\beta = 60^{\circ}$; $T_c = 0.04$.

(b)  Climb condition: $\alpha = 6^{\circ}$; $\beta = 40^{\circ}$; $T_c = 0.11$.

power off
power on
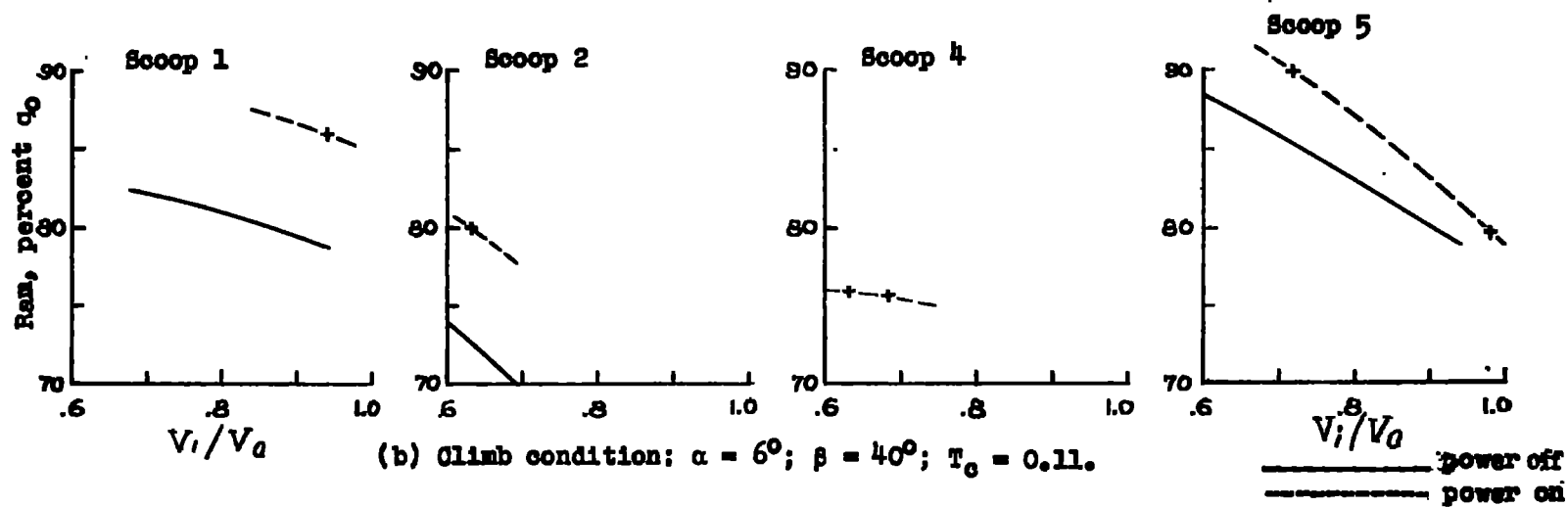
Figure 29.- Effect of slipstream on ram at the carburetor.

Fig. 29

Scoop 5          Inside of duct bend          Scoop 2

540          52.0

56.0          -54.0

$V_1/V_0 = 0.40$    Ram = 91.2%$q_0$
$Q/V_0 = 0.07$    $q_0 = 60.1$ mm alcohol
$\alpha = 1°$   propeller off

$V_1/V_0 = 0.40$    Ram = 91.0%$q_0$
$Q/V_0 = 0.08$    $q_0 = 59.5$ mm alcohol
$\alpha = 1°$   propeller off

58.0          54.0

60.0          56.0

58.0

$V_1/V_0 = 0.40$    Ram = 96.3%$q_0$
$Q/V_0 = 0.07$    $q_0 = 60.3$ mm alcohol
$\alpha = 1°$    $\beta = 60°$    $T_c = 0.04$
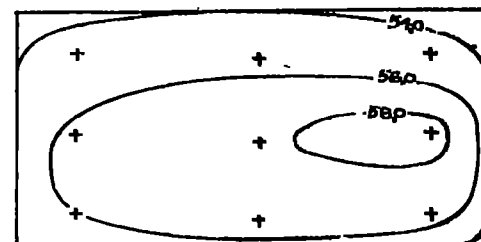
$V_1/V_0 = 0.40$    Ram = 93.8%$q_0$
$Q/V_0 = 0.08$    $q_0 = 59.3$ mm alcohol
$\alpha = 1°$    $\beta = 60°$    $T_c = 0.04$

26.0
28.0
30.0
32.0
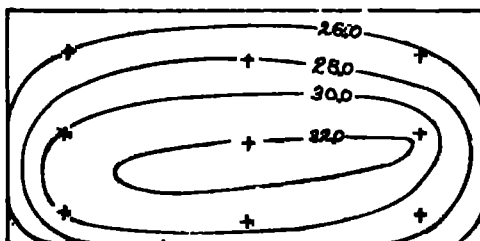
$V_1/V_0 = 0.80$    Ram = 86.9%$q_0$
$Q/V_0 = 0.15$    $q_0 = 31.7$ mm alcohol
$\alpha = 6°$    $\beta = 40°$    $T_c = 0.11$

Figure 30.- Effect of slipstream on total pressure, $H_c$, with straight and twisted scoops.
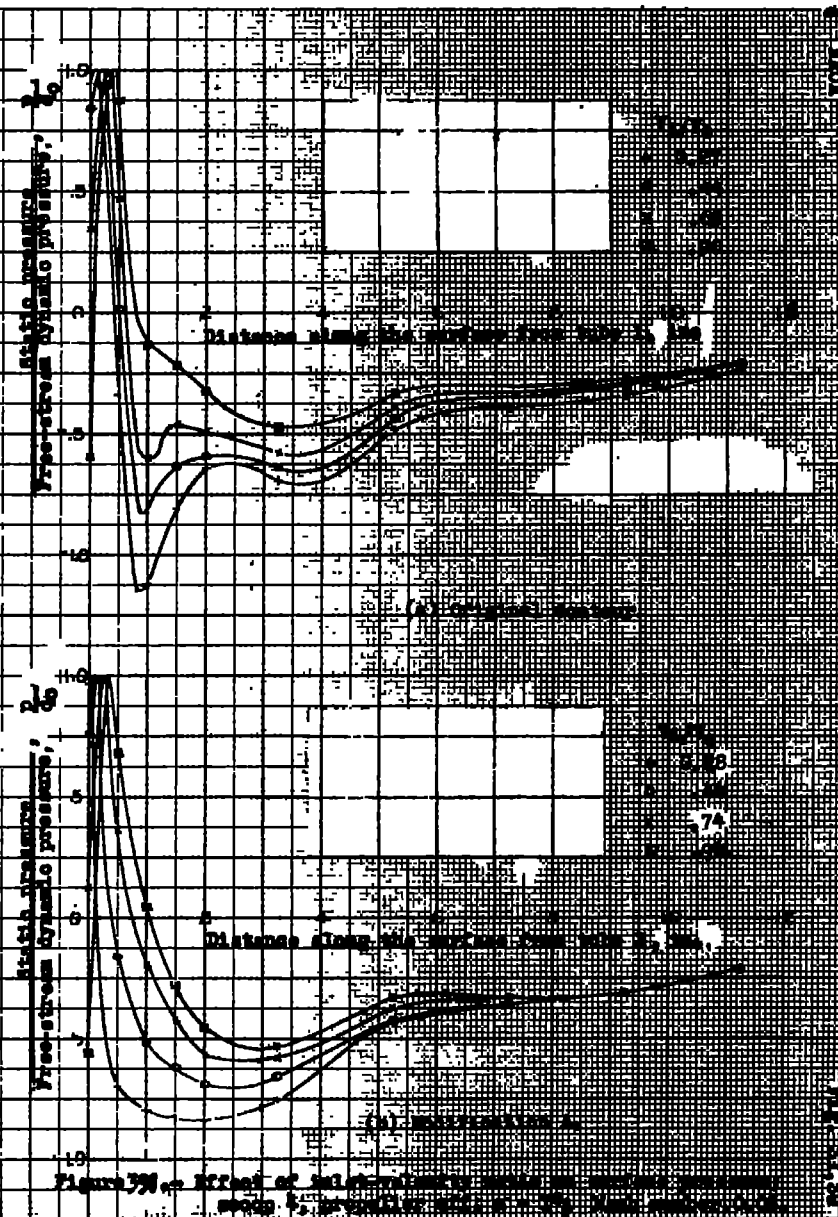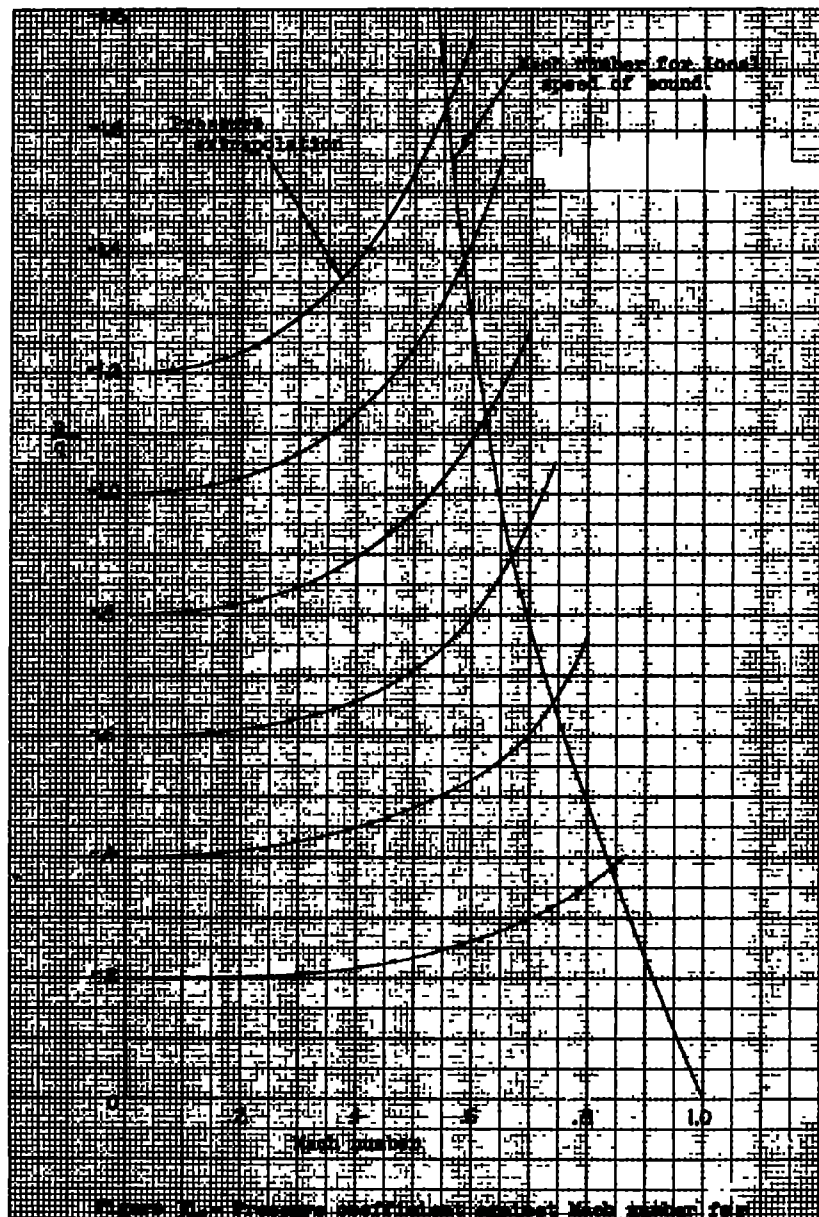Values on contours are in millimeters of alcohol.

Fig. 30

Mach number for local
speed of sound

Distance along the surface from nose, in.

(b) Suction pressure.

Distance along the surface from nose, in.

(a) Distribution.

Figure 73.— Effect of ...
... speed.

Figure ... Graphical method for
determining critical speed.

Figure 32.- Effect of $V_1/V_0$ on the angle of attack of the inlet lip.

Original contour ————
Modification A —·—·—
" B ············
" C —··—··—
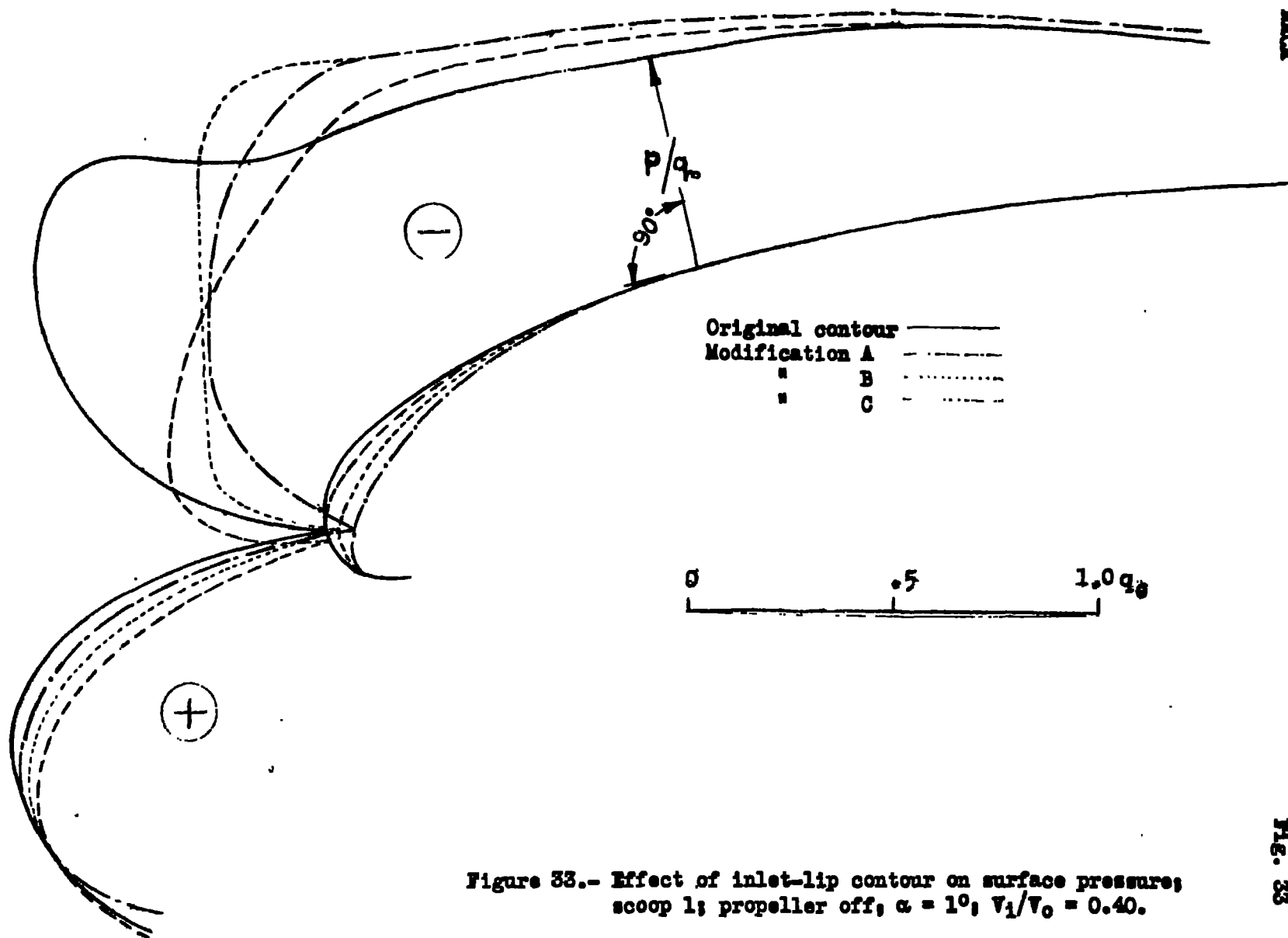
Figure 33.- Effect of inlet-lip contour on surface pressure;
scoop 1; propeller off, α = 1°, $V_1/V_0$ = 0.40.

Fig. 33

Original contour ——————
Modification A —·—·—·—
       "        B ————

0            .5           1.0 $q_0$
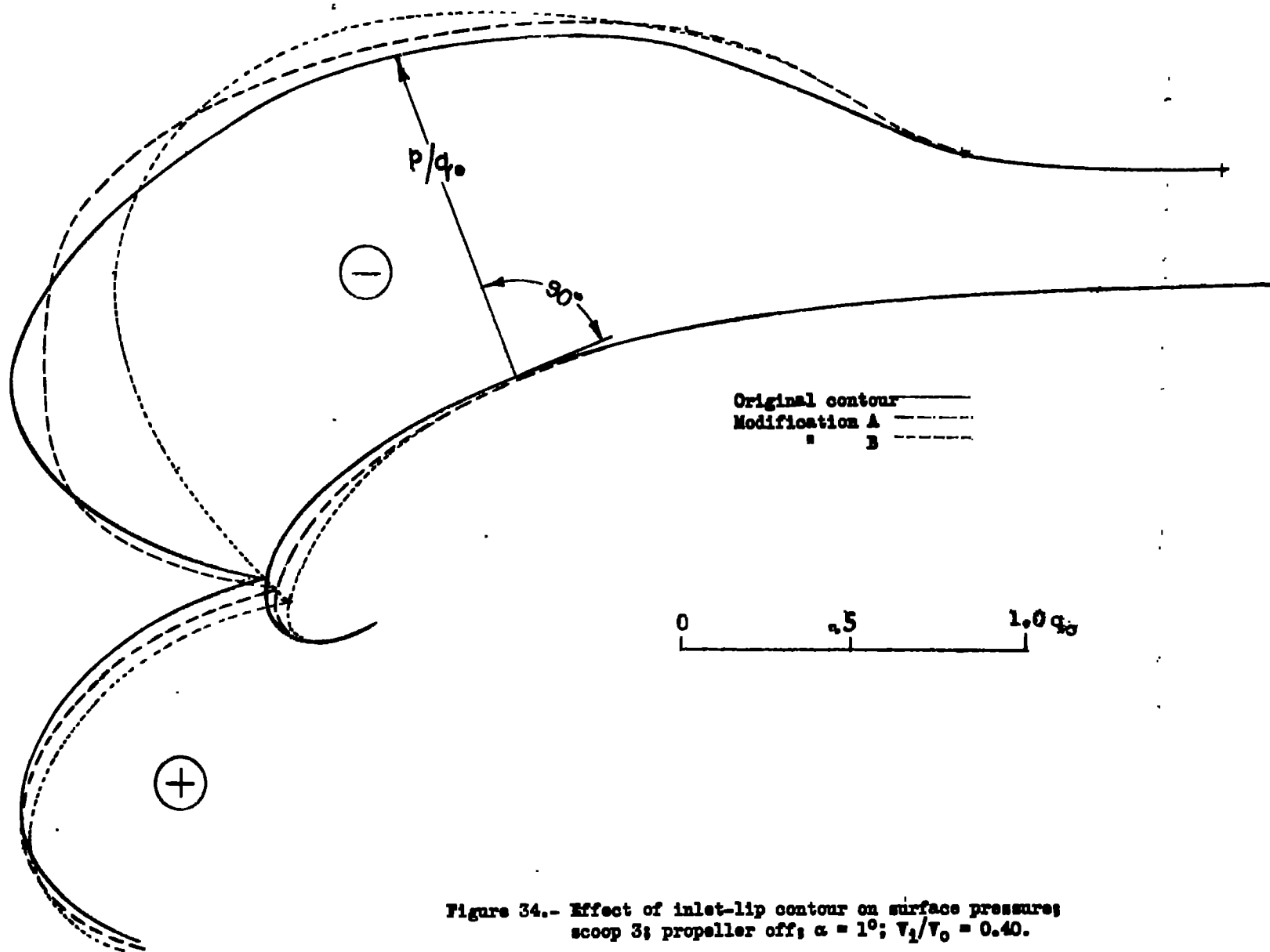
Figure 34.- Effect of inlet-lip contour on surface pressure;
scoop 3; propeller off; $\alpha = 1°$; $V_i/V_0 = 0.40$.

FIG. 34.

$P/q_o$

90°

⊖
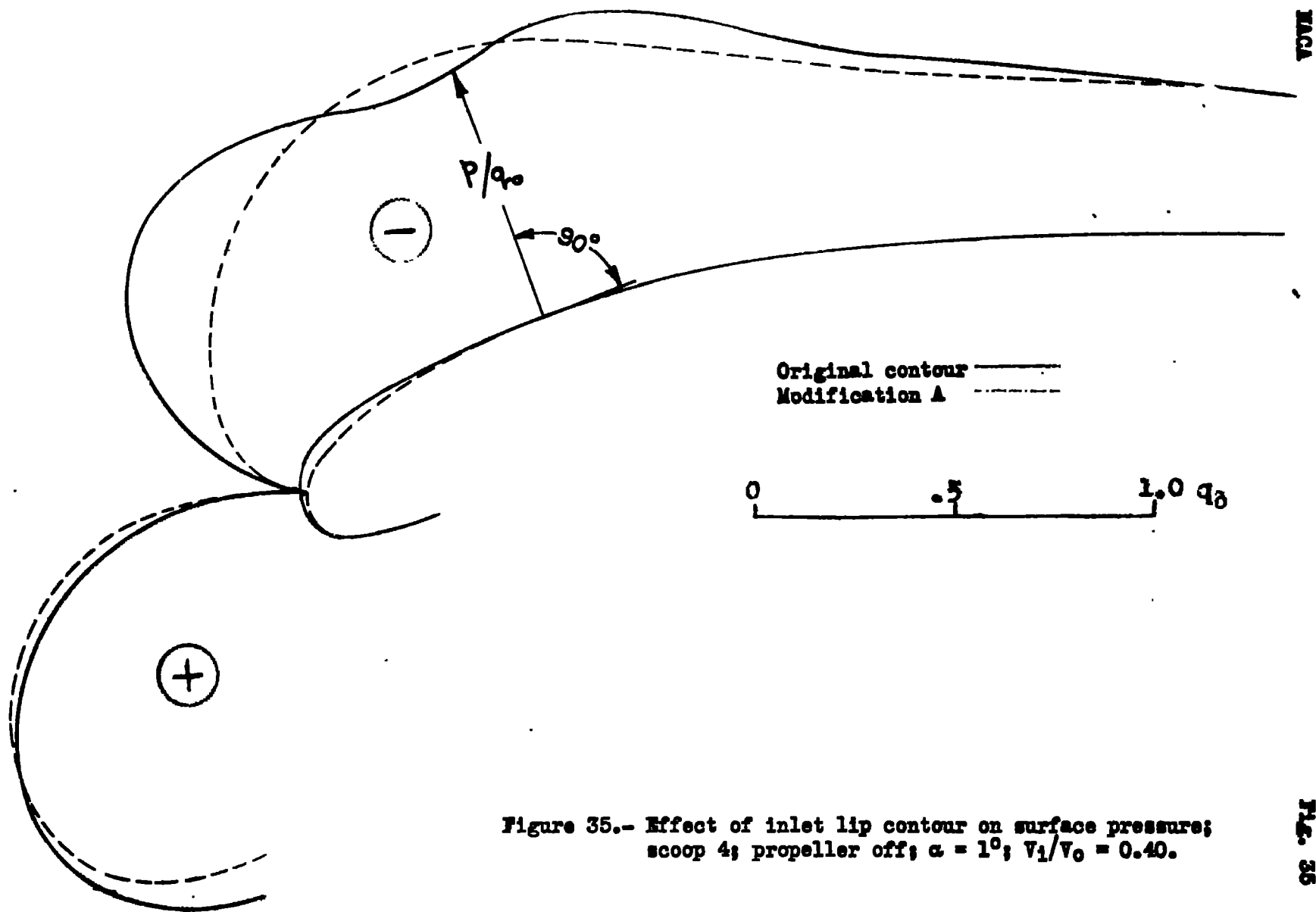
⊕

Original contour ———
Modification A ———·——

0      .5      1.0 $q_\delta$

Figure 35.- Effect of inlet lip contour on surface pressure;
scoop 4; propeller off; $\alpha = 1^\circ$; $V_1/V_0 = 0.40$.

Fig. 35

$p/q_0$

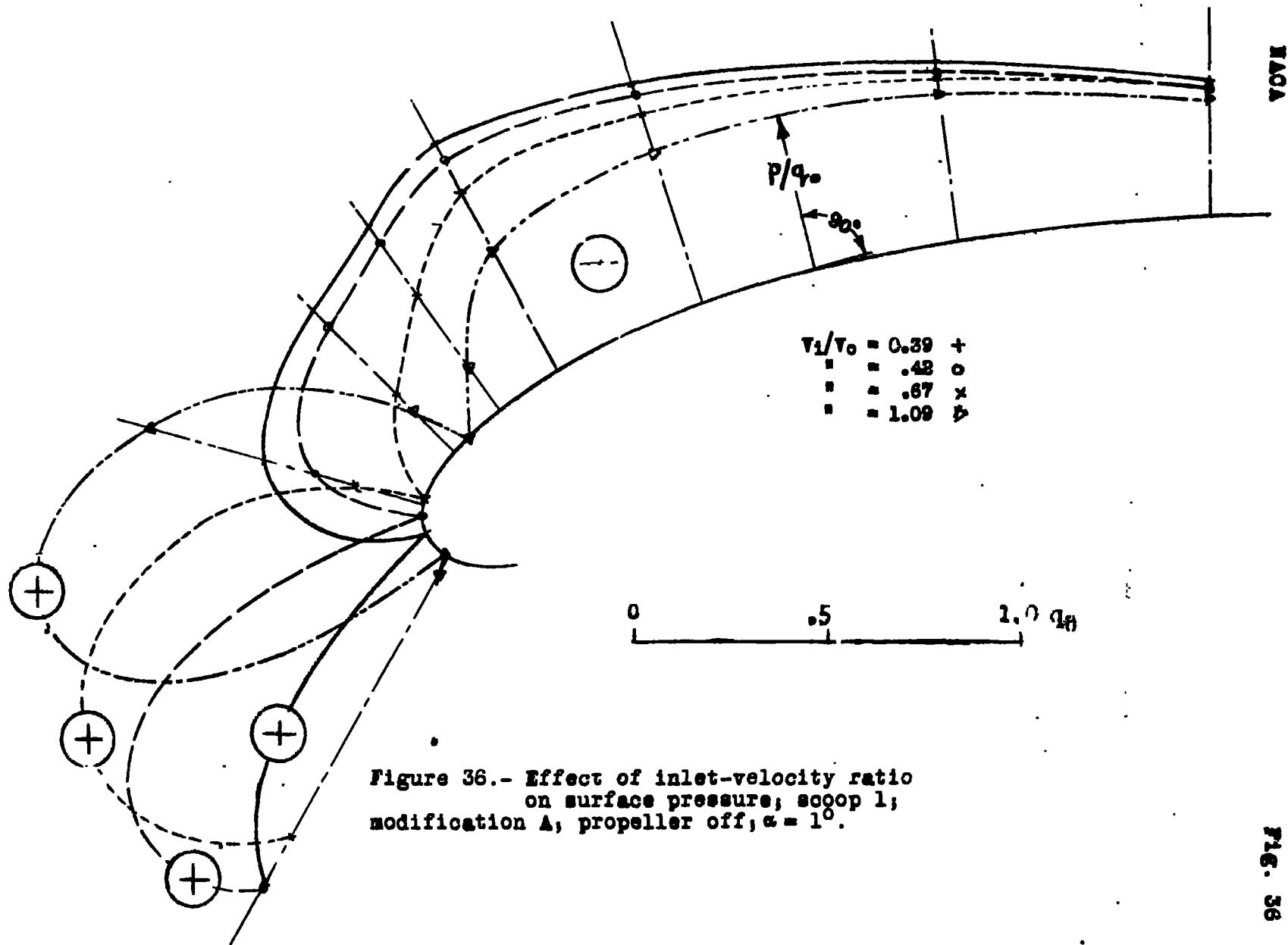$\theta_0$

$V_1/V_0 = 0.39$ +

" = .42 ○

" = .67 ✕

" = 1.09 ▷

0 .5 1.0 $q_0$
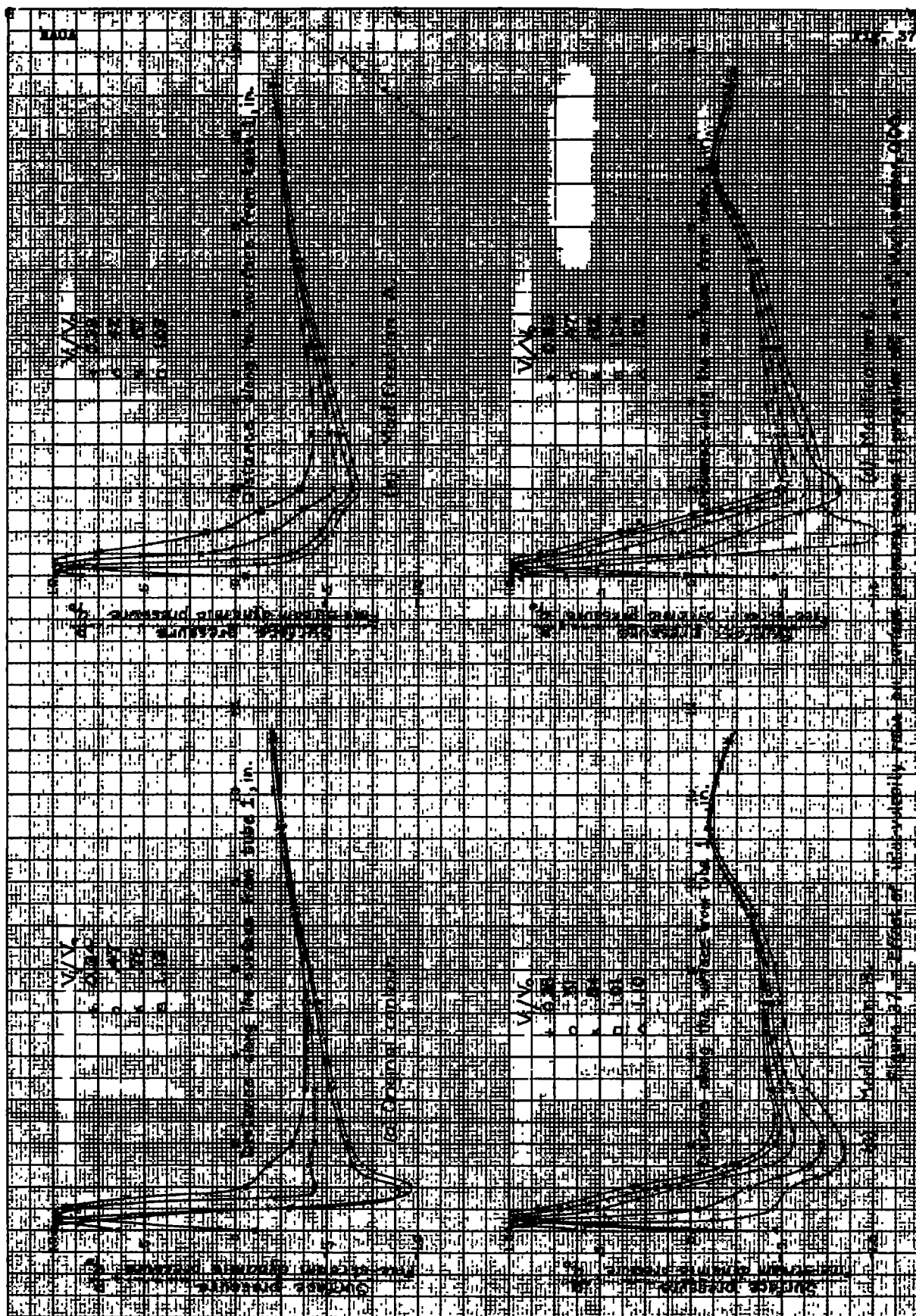
Figure 36.- Effect of inlet-velocity ratio
on surface pressure; scoop 1;
modification A, propeller off; $\alpha = 1^\circ$.

Fig. 36

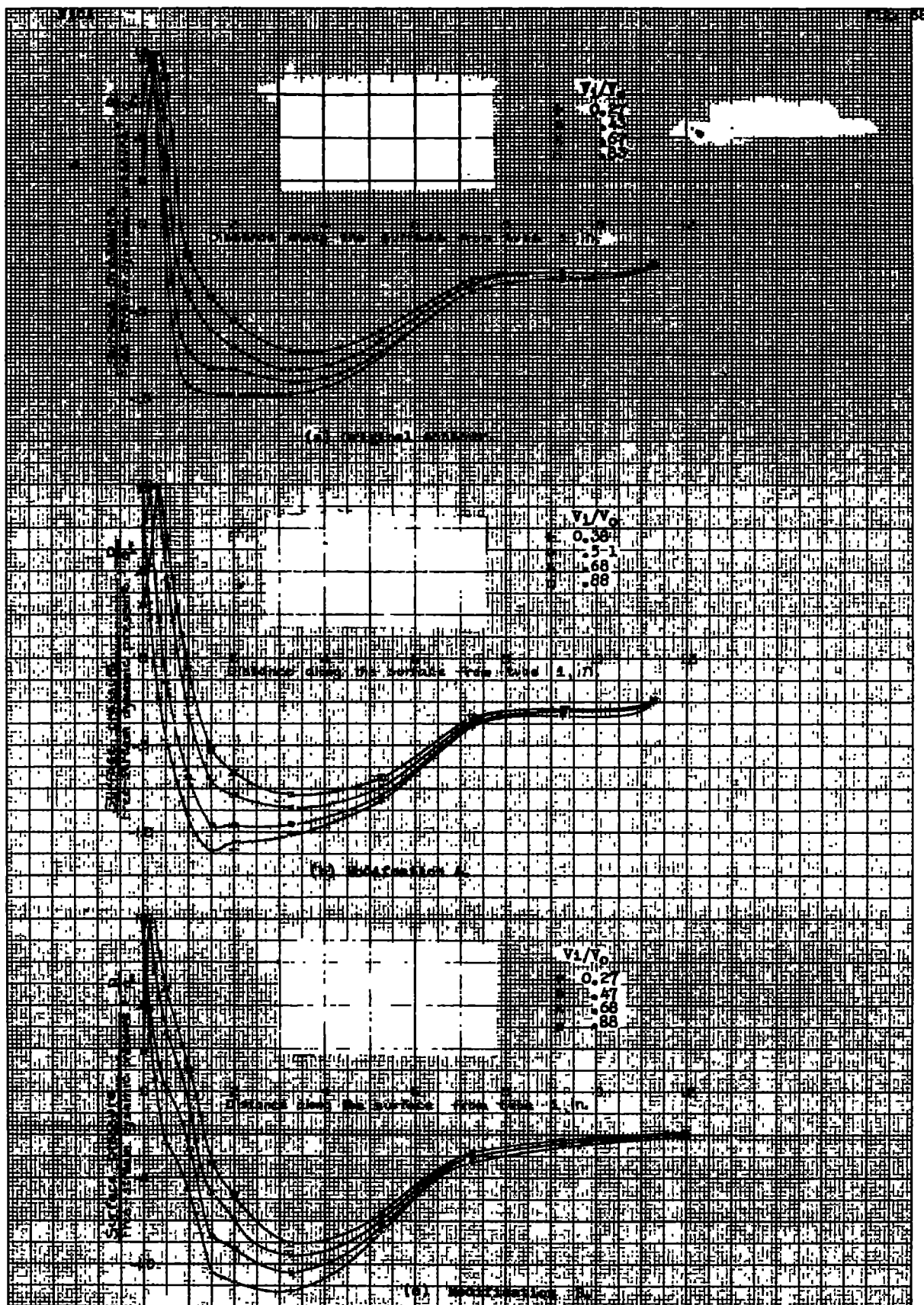(a) Original scoop.

(b) Modification 1.

(c) Modification 4.

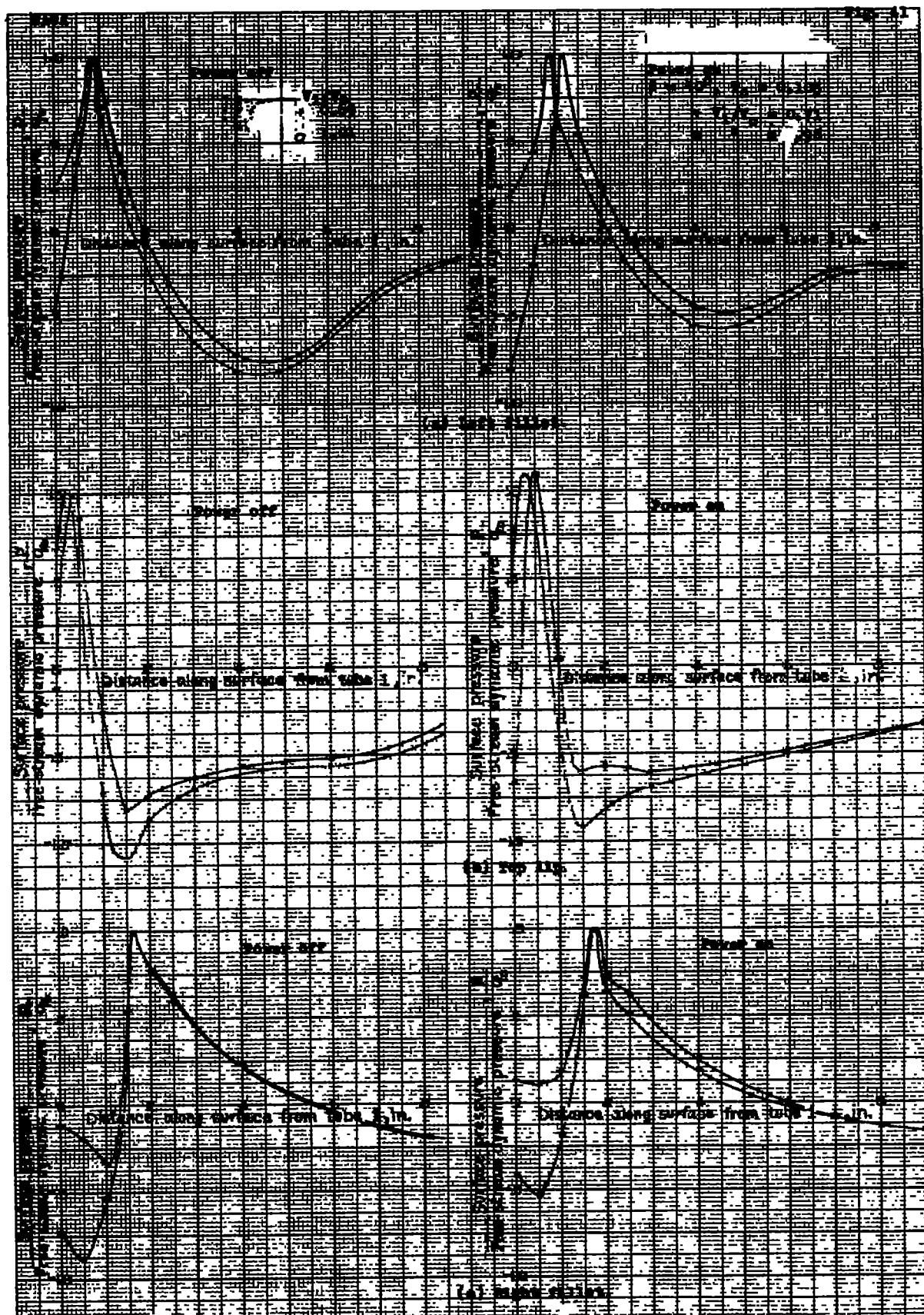Figure 38. Effect of inlet-velocity ratio on surface pressure; scoop 3; propeller off; $\alpha = 1°$; Mach number, 0.08.

Fig. 41

Figure 41.- Effect of inlet-velocity ratio and propeller slipstream on surface pressure; scoop 5, α = 6°, climb condition; Mach number 0.08.